AD NUMBER: AD0357975
CLASSIFICATION CHANGES
TO: Confidential (Formerly Restricted Data)
FROM: Secret (Formerly Restricted Data)
AUTHORITY
30 Nov 1961, DASA

[redacted]

WT-1434

This document consists of 56 pages.

No. [redacted] of 200 copies, Series A

OPERATION

PLUMBBOB

NEVADA TEST SITE

MAY-OCTOBER 1957

Project 5.5

IN-FLIGHT STRUCTURAL RESPONSE of an F-89D AIRCRAFT to a NUCLEAR DETONATION (U)

[redacted] (Changed to [redacted]

By authority of DASASC-3 memo, 30 Nov 61

By [redacted] Date 4 Dec 61

Issuance Date: March 22, 1960

HEADQUARTERS FIELD COMMAND
DEFENSE ATOMIC SUPPORT AGENCY
SANDIA BASE, ALBUQUERQUE, NEW MEXICO

[redacted]

Inquiries relative to this report may be made to

Chief, Defense Atomic Support Agency
Washington 25, D. C.

When no longer required, this document may be destroyed in accordance with applicable security regulations.

DO NOT RETURN THIS DOCUMENT

AEC Technical Information Service Extension
Oak Ridge, Tennessee

[redacted]

(5) Aeronautical Systems Div.,
Air Force Systems Command,
Wright-Patterson AFB, Ohio.

(18) AEC
(19) WT-1434
(21) Report No.

OPERATION PLUMBBOB - PROJECT 5.5 [U].

(6)

IN-FLIGHT STRUCTURAL RESPONSE of an F-89D AIRCRAFT to a NUCLEAR DETONATION (U).

(8)

FOREIGN ANNOUNCEMENT AND DISSEMINATION OF THIS REPORT BY DDC IS NOT AUTHORIZED.

(9) Final rept.,

(10)

by
G. Stalk, [redacted]
R. E. Gee, [redacted]
and J. P. Bednar, [redacted]
and the Staff of
~~Northrop Aircraft, Inc.~~
~~Hawthorne, California~~

(11) 22 Mar 60,

Wright Air Development Center
Air Research and Development Command
United States Air Force
Wright-Patterson Air Force Base, Ohio

U.S. GOVERNMENT AGENCIES MAY OBTAIN COPIES OF THIS REPORT DIRECTLY FROM DDC. OTHER QUALIFIED DDC USERS SHALL REQUEST THROUGH

Director
Defense Atomic Support Agency
Washington, D. C. 20301

[redacted]

ABSTRACT

The primary objective of Project 5.5 was to determine the structural response of the F-89D aircraft in flight to the blast and thermal effects of a nuclear detonation. The recorded data will be used to correct or verify the F-89J Weapons System Capability Study and to further define the F-89J weapon-delivery capability. Use of the F-89D test aircraft to evaluate the F-89J analysis was valid because of the structural similarity of the two models.

To accomplish the objective, the test aircraft was instrumented to measure the overpressure, gust (dynamic-pressure wave), and thermal inputs together with the aircraft response to these inputs. The aircraft was positioned at predetermined points in space in the vicinity of nuclear detonations. The positions selected were not necessarily representative of delivery maneuvers but were at points where the combination of dynamic loads and steady state loads would approach the design limit load.

For each shot except John the aircraft was positioned to receive a high response on the most critical structual member for the particular orientation and gross weight used without exceeding the 5 rem-per-mission limit for maximum nuclear radiation exposure to the aircrew. The range of maximum structural response was 70 to 100 percent of design limit load. In all events except Shot John the aircraft was positioned at various slant ranges from ground zero and was flying in a steady-state 1.0 g level flight condition at shock arrival. On Shot John authorization was granted to exceed the 5 rem-per-mission limit but remain within the 35-rem-total-accumulated dosage for the aircrew participating in this event. Shot John was a delivery of an air-to-air weapon (MB-1), containing a nuclear warhead, from an F-89J aircraft with the Project 5.5 F-89D aircraft flying side-by-side formation. At the time of launch, the Project 5.5 aircraft and the delivery aircraft banked in opposite directions performing a typical escape maneuver as determined by the F-89J capability study.

The aircraft successfully participated in 14 events with yields ranging from 0.1 kt to 74.1 kt. Maximum nuclear dosage received by the aircrew occurred in Shot John where the pilot received 3.55 rem and the project flight engineer received 2.44 rem. The maximum free-stream overpressure measured was 0.51 psi during Shot Shasta and the maximum gust loading occurred during the Shot Boltzmann participation where 84 percent design limit load was recorded at Wing Station 267.

From the participation of the F-89D aircraft in Operation Plumbbob, it can be concluded that the response of the F-89J to the blast associated with a nuclear detonation produces higher wing loads than predicted analytically in Reference 1. Therefore, that report should be corrected to reflect the information obtained by this project.

FOREWORD

This report presents the final results of one of the 46 projects comprising the military-effects program of Operation Plumbbob, which included 24 test detonations at the Nevada Test Site in 1957.

For overall Plumbbob military-effects information, the reader is referred to the "Summary Report of the Director, DOD Test Group (Programs 1–9)," ITR–1445, which includes: (1) a description of each detonation, including yield, zero-point location and environment, type of device, ambient atmospheric conditions, etc.; (2) a discussion of project results; (3) a summary of the objectives and results of each project; and (4) a listing of project reports for the military-effects program.

CONTENTS

Chapter 1
INTRODUCTION

1.1 OBJECTIVES

The primary objective of Project 5.5 was to determine the structural response of the F-89D aircraft in flight to the blast and thermal effects of a nuclear detonation. The recorded data will be used to correct or verify the method of analysis used for the F-89J Weapons System Capability Study (Reference 1). In addition, the project will provide basic research data for design of future USAF aircraft.

1.2 BACKGROUND

Since the original tests of nuclear weapons, considerable effort has been made to determine the effects of the detonations on aircraft systems. Actual aircraft participation in the earlier nuclear tests was quite limited because of a lack of knowledge of weapon characteristics and their effects on the aircraft system. In order to define accurately the safe delivery capabilities of present-day and future aircraft, the Air Force initiated a research and development program consisting of theoretical analysis and experimental tests.

Initial work of this type consisted of approximate and hypothetical studies performed during Operations Crossroads and Sandstone. Following this, Massachusetts Institute of Technology (MIT) was contracted to develop theories to predict the effects of nuclear explosions on aircraft structures.

Thirteen aircraft participated in Operation Greenhouse to gather data for the verification or correction of the MIT theoretical study. Participation in Operations Ivy, Upshot-Knothole, and Castle provided further data for the verification of the MIT theories as well as determination of the delivery capabilities of the B-36 and B-50 aircraft.

As the analytical methods of predicting weapon characteristics became more reliable, aircraft participation in nuclear tests became more extensive. Data obtained from participation in Operations Teapot and Redwing is being used to define the delivery capabilities of the F-84, F-101, B-47, B-52, B-57, and B-66 aircraft. Problem areas concerning thermally induced stresses, lethal envelopes, side gust loading, and secondary effects on aircraft components such as radomes, honeycomb skin sections, and engines were also investigated in Operations Teapot and Redwing.

The development of the F-89J weapon system incorporated the capability for delivery of an air-to-air rocket with a nuclear warhead (MB-1 weapon) from an interceptor aircraft. In conjunction with this, a study was initiated to define the safe delivery and escape maneuvers for effective delivery of the MB-1 weapon. Plumbbob Project 5.5 was a continuation of this program. The participation schedule for this project is shown in Table 1.1.

Since the instrumentation necessary for adequate response data had been previously installed, F-89D Serial No. 51-411 was selected as the test vehicle for participation in Operation Plumbbob. Use of the data measured by the F-89D test aircraft to evaluate the F-89J analysis was valid because structural differences existed only in the wing-tip region where the tip-pod fittings and attachment to the spars were stronger on the F-89J to permit the installation of heavier tip pods. This strength was only increased locally, and the general wing structural characteristics remained unchanged.

The F-89J Weapons System Capability Study (Reference 1) indicated that at altitudes above 20,000 feet the aircraft capabilities for delivery of an MB-1 weapon were limited by the allowable nuclear dosage to which the crew might be subjected. Since it was not desirable to expose the crew to the nuclear-dosage levels required to evaluate the nuclear barriers, the scope of this project was limited to an evaluation of the aircraft

TABLE 1.1 GENERAL SHOT DATA

Date	Shot	Approximate Time, Pacific Daylight Time	Burst Height and Support	Ground Elevation	Yield		
					Preshot Positioning	Preshot Design	Postshot Actual
			ft	ft	kt	kt	kt
28 May 1957	Boltzmann	0455	500, tower	4,200	12.5	11.0	11.5
2 June 1957	Franklin	0455	300, tower	4,000	4.0	2.0	0.138
18 June 1957	Wilson	0445	500, tower	4,230	20.0	8.0	10.3
24 June 1957	Priscilla	0630	700, balloon	3,080	45.0	40.0	36.6
5 July 1957	Hood	0440	1,500, balloon	4,230	110.0	60.0	74.1
15 July 1957	Diablo	0430	500, tower	4,470	25.0	11.0	18.7
19 July 1957	John	0700	19,110, rocket	—	1.9	1.7	1.73
24 July 1957	Kepler	0455	500, tower	4,307	15.0	11.0	10.3
25 July 1957	Owens	0630	500, balloon	4,212	15.0	6.0	9.6
7 August 1957	Stokes	0620	1,500, balloon	4,180	22.0	10.0	19.0
18 August 1957	Shasta	0500	500, tower	4,380	20.0	11.0	16.8
23 August 1957	Doppler	0530	1,500, balloon	4,186	15.0	12.5	10.7
30 August 1957	Franklin Prime	0540	750, balloon	4,186	6.0	2.0	4.7
31 August 1957	Smoky	0530	700, tower	4,480	60.0	45.0	43.71

structural response over the altitude range where the capability of the aircraft is controlled by wing loads. Related nuclear-dosage information obtained by Plumbbob Projects 2.5 and 2.9 will be used to verify the overall nuclear analysis for the F-89J Weapon System Capability Study.

1.3 THEORY

The determination of the effects of a nuclear detonation on the aircraft structure and crew required consideration of the following weapon phenomena: (1) overpressure associated with the shock wave; (2) gust associated with the shock wave; (3) time of shock arrival; (4) triple-point path; (5) nuclear radiation; (6) rise of the radioactive cloud; and (7) thermal radiation from the fireball.

1.3.1 Overpressure. The overpressure associated with the shock wave at any given point in space was computed from the free-air overpressure curve based on the M-Problem and the modified α correction for altitude effects as contained in Reference 9. The overpressure for the reflected shock was computed by the same method, using the slant range from a mirror image of the burst below the reflecting surface.

If the impingement angle of the shock wave is normal or nearly normal to the airfoil chord plane, the pressure field is diffracted as it envelopes the airfoil. This diffraction

causes a pressure differential across the section for a finite time and can produce a structural response in addition to that produced by the gust.

A dynamic analysis was conducted on the F-89 wing and horizontal tail to account for diffraction. This analysis provided theoretical time-history plots of incremental shear, moment, and torsion for various stations on the wing, stabilizer, and fuselage. The maximum values of each type of load at a particular station are then added algebraically to obtain the complete gust induced incremental load at any one station. These theoretical values of the combined loads were then compared between stations to ascertain the most critical station along a particular structural member of the aircraft.

Theoretical analysis established that the critical areas because of the crushing effects of overpressure were the engine-cowl doors. The doors were of conventional skin-stringer construction with frames at the ends. The maximum-permissible net-static-pressure rise because of overpressure was obtained by subtracting the steady-state pressure from the maximum-permissible pressure. By this method an allowable limit overpressure of 1.36 psi was calculated. The analysis assumed a constant static pressure applied to the surface. A reflection of pressure such that the resultant pressure is approximately twice the incident overpressure occurs when the shock-wave impingement angle is normal or nearly normal to the surface. Since the engine-cowl doors are located on the under surface of the fuselage, it was assumed that the incident pressure was magnified by a factor of 2.0 and the resultant pressure was acting on the surfaces.

The allowable overpressure calculated was a limit value; however, permanent buckling or damage would not occur until the ultimate value is reached, i. e., 1.5 times the limit value of 1.36, or 2.04 psi. For the following reasons, the ultimate value of 2.0 psi was established as the allowable which permits an incident overpressure of 1.0 psi: (1) the structure is subjected to this load for an extremely short period of time; (2) because of the factor of safety involved in the analysis, any damage would probably be restricted to local buckling; (3) loss of the component would not cause loss of the aircraft.

1.3.2 Gust. The peak gust velocity associated with the shock wave at any point in space was obtained from the predicted overpressure and the normal shock-wave relations as given by the Rankine-Hugoniot equations. The method used for predicting the overpressure is defined in Section 1.3.1.

A dynamic-load analysis was conducted by the method used for Reference 1 and presented in detail in Reference 3. This method is essentially the same as that contained in Reference 2. A brief general discussion of the dynamic analysis is contained in the following paragraphs.

Equations were derived to calculate dynamic wing loads for a 1-ft/sec gust normal to the wing chord plane, yielding a solution which gave unit dynamic loads that varied linearly with gust velocity. These loads were dependent upon the gust input shape, air density, and the airplane forward velocity, wing angle of attack and weight distribution. The shape of the gust input, which was the time-history plot of overpressure during and after the passage of the shock front, and the time duration of the positive pressure phase varied with weapon yield, slant range, and altitude. For this reason, the unit dynamic loads were calculated for eight gust input shapes, three altitudes, three weight configurations, and two aircraft Mach numbers to account for the range of conditions to be tested.

To account for the initial wing angle of attack, the maximum density change associated with the shock wave, and the change in forward velocity of the aircraft because of a longitudinal component of the gust velocity, a correction factor (K) was computed by a method presented in Reference 3. The product of the K factor and the gust component

normal to the wing chord plane (U_{e_z}) resulted in an effective gust velocity (KU_{e_z}), which when multiplied by the unit loads for the above parameters, yielded the total incremental dynamic gust loads. The total loads on the structure consisted of the algebraic sum of the steady-state loads on the structure prior to shock arrival and the total incremental dynamic load.

The wing loads calculated by the dynamic analysis are affected by the aircraft pitch response to the gust input. Since this aircraft response is primarily dependent on the horizontal tail loads, these loads were calculated for use in the analysis. Based on the recommendation of Reference 2, the horizontal tail was assumed to be 100 percent effective, i. e. , no downwash because of the gust input. For the wing analysis, the aft fuselage and horizontal tail were assumed rigid to simplify computation of the aircraft pitch response, since the flexibility of these components was considered to produce a negligible effect on the wing loads. However, a separate analysis was conducted to calculate the loads on the fuselage and horizontal tail, which included the effect of fuselage and horizontal tail flexibility.

Time histories of shear, bending moment, and torsion at each selected wing station were obtained from this analysis. Since the design-wing-load envelopes for the F-89 consist of combined loads, i. e. , bending moment versus torsion, and shear versus torsion, the load combinations obtained at a given time were compared with the wing-load envelopes to determine their relationship to the design loads. The aircraft position was then based on the combined loads rather than individual loads such as bending moment alone or torsion alone.

Side loads on the vertical tail were calculated from the rigid-body sharp-edged gust equation of Reference 4, using the side component of the gust velocity. It was assumed that the product of the alleviation factor and dynamic-magnification factor was equal to one. Dynamic magnification factor is defined as that factor which accounts for the increase in incremental, rigid-body gust response because of the inertial overshoot of the responding structural member; alleviation factor accounts for aerodynamic and structural damping characteristics associated with the gust induced excitation. Previous analysis on other structural components of the F-89 indicated that this assumption was generally reasonable or conservative. The analysis conducted for Reference 1 indicated a low-load level on the vertical tail; therefore, additional refinement of the analysis was not warranted.

1.3.3 Time of Shock Arrival. The time of shock arrival at any given point in space was computed by an empirical equation derived from results obtained in Operation Redwing:

$$t_{sa} = (S/C_{ave}) - 0.7W^{1/3} \qquad (1.1)$$

Where: S = Slant range from burst point to any given point in space, t.

C_{ave} = Average speed of sound between the speed of sound at the burst point and the speed of sound at the point in space, ft/sec.

W = Weapon yield, kt.

Time of shock arrival for the reflected shock was computed by the same method, using the slant range from a mirror image of the burst below the reflecting surface.

1.3.4 Triple Point Path. Triple point paths were established from Armed Forces Special Weapons Project (AFSWP) experimental data which had been scaled to 1-kt, sea-level conditions. The information from the basic curves was rescaled to the pertinent yield conditions by modified Sachs scaling.

The triple point path is produced by detonations creating an initial blast wave and a reflected wave. In the case of a nuclear detonation situated near the earth's surface, that part of the initial blast wave moving downward strikes the ground and creates a reflected wave which then moves upward and outward following behind the initial shock front. However, the reflected shock wave moves faster because it travels through a region which is hotter and more dense than the ambient atmosphere because of the passage of the initial wave. Under appropriate conditions, the reflected shock overtakes and merges with the initial shock wave forming a single shock front referred to as the Mach stem. The point of merger of the initial and reflected shock waves into the Mach stem is called the triple point path and first occurs near the ground. As altitude increases, it forms at further distances measured from the point of detonation to the triple point path.

1.3.5 Nuclear Radiation. Computation of the nuclear radiation dosage was based on the methods presented in References 5 and 6. The latter method accounts for radiation emitted by the radioactive cloud and is a function of the slant range between the cloud and the aircraft. This was an important consideration when the aircraft was approaching ground zero at the time of shock arrival. The total nuclear radiation consisting of the instantaneous dosage at burst time and the dosage accumulated was calculated by numerical integration over the aircraft flight path. The instantaneous dosage is the summation of the biological dose from neutrons and the fission-product gamma dosage computed from data presented in Reference 6. The biological dose from neutrons is given by the equation:

$$\text{Neutron Dose} = \frac{I_0 \, W \, f(g/cm^2)}{X^2} \tag{1.2}$$

Where:
I_0 = Source strength term, usually called the intercept
W = Yield in kilotons
$f(g/cm^2)$ = Transmission factor
X = Slant range in yards from burst point to receiver.

The intercept, I_0, and transmission factor, $f(g/cm^2)$ are both functions of weapon design. The fission-product gamma dosage is given by the equation:

$$\text{Gamma Dose} = \frac{I_0 \, W \, f(W) \, f(g/cm^2)}{X^2} \tag{1.3}$$

Where:
I_0 = Intercept value
W = Yield in kilotons
$f(W)$ = Hydrodynamic scaling factor
$f(g/cm^2)$ = Transmission factor
X = Slant range in yards

Furthermore, a reduction factor 0.375 was applied to the fission product gamma dosage. This factor included a correction of 0.75 for adjustment of data presented in Reference 6 and also included a factor of 0.5 to account for radiation attentuation by the aircraft structure.

For each event except Shot John, the maximum nuclear dosage permitted was 5 rem with a total of 35 rem for the series. Since this limitation proved to be restrictive for Shot John, authorization was granted to exceed the 5 rem limit but remain within the 35 rem total accumulated dosage for the aircrew participating in this event.

1.3.6 Rise of Radioactive Cloud. Data for cloud rise was obtained from Figures 27 and 28 of Reference 7 and from Reference 6, respectively. This provided the method for determining the slant range between the cloud and the aircraft at any time after burst. Since the aircraft was positioned to be short of ground zero for several events, the cloud rise proved to be an important factor in the nuclear radiation limitations because of the radiation emitted from the cloud.

The amount of cloud rise, H, was calculated from the equation:

$$\Delta H = 190\, W^{0.2}\, t^{0.8} \tag{1.4}$$

Where: ΔH = Rise of cloud center in feet

W = Yield in kilotons

t = Time in seconds

This relationship was empirically derived from curves of cloud height versus time for Operation Teapot during the time interval from 10 seconds to 2 minutes. Within this time period the average deviation of the equation from the Operation Teapot data was ±10 percent.

1.3.7 Thermal Radiation. Thermal radiation was computed by the method presented in Reference 8. The expression for total thermal energy impinging normal to a horizontal surface may be written:

$$Q_{rec} = Q_n \left[F_V (T_V \cos\Theta + T_V \alpha\gamma) + F_{IR} (T_h\, T_w \cos\Theta + T_h\, T_w \alpha\gamma) \right] \Delta \tag{1.5}$$

Where: Q_{rec} = Thermal radiation at the receiver in cal/cm^2

Q_n = Thermal radiation from the source normal to the receiver in cal/cm^2

F_V = Fraction of thermal energy in the visible region

T_V = Fractional transmission due to scattering in the visible range

Θ = Angle between the normal to the burst and the normal to a horizontal receiver

T_V = Fractional transmission of reflected radiation in the visible region

α = Surface albedo

γ = Ratio of reflected to direct energy in a vacuum

F_{IR} = Fraction of thermal energy in the infrared range

T_h = Fractional transmission due to scattering in haze layer for entire spectrum for direct radiation

T_w = Fractional transmission due to water vapor absorption in the infrared range

T_h = Fractional transmission due to scattering in the haze layer over the entire spectrum for reflected radiation.

T_w = Fractional transmission in the infrared region due to water vapor absorption for reflected radiation

Δ = Fraction of total thermal energy released in the fireball.

The equation for the incident thermal flux was modified for the case of a flat plate normal to the direct radiation. This neglected any thermal relief due to incidence angle and assumed the surface being analyzed to be perpendicular to the line of sight between the surface and the fireball. This modification was utilized because the critical component was the elevator, and movement of this surface would vary the angle of incidence. The skin-temperature rise resulting from the incident thermal flux was evaluated by the method presented in Reference 2, which accounts for aerodynamic cooling of the heated surface. This computation involves a numerical integration of thermal radiation input minus heating loss through the boundary layer where this heat loss is a function of airspeed, density, and distance back from the leading edge in the direction of airflow. The entire elevator structure was assumed to be at adiabatic wall temperature prior to time zero.

Analysis conducted prior to the test operation indicated that for yields greater than 20 kt excessive temperatures would be experienced on nonmetallic external parts and on thin-skinned components. This analysis assumed a dirty aluminum condition with an absorptivity of 0.75. To alleviate this problem and permit positioning for the desired magnitude of dynamic loads, the non-metallic parts were coated with a highly reflective white material (Minnesota Mining and Manufacturing Company's EC-1561). In addition, a white gloss paint was applied to the following thin-skinned components: rudder; engine cowl doors; and lower surfaces of the elevators, horizontal stabilizers, ailerons, and landing flaps. In order to obtain the desired temperature data to correlate with analysis, certain small local areas which contained thermocouple installations were left bare, or were painted white or black. In this configuration, the temperature analysis was based on an absorptivity of 0.25 for the white gloss paint and 1.0 for the black test panels.

1.4 SCOPE

Because of the limited number of tests available during Operation Plumbbob, it was not practical to obtain test data over the entire range of conditions used in the F-89J Weapons System Capability Study. Therefore, test conditions were selected to provide the best possible data for the evaluation of the dynamic wing analysis. Selection of the test conditions was made by considering the desired input and the operational feasibility of obtaining these conditions.

The initial series of test conditions contained a minimum number of variables affecting the dynamic loads, in order to verify the reliability of test results. The aircraft was positioned to receive the gust from directly below, head on, or tail on. To minimize

changes in aerodynamic data, an aircraft speed range of Mach 0.755 to 0.78 was used because the major aerodynamic parameters were essentially constant in this Mach range.

After reliable data was obtained to evaluate the basic dynamic analysis, the test conditions were changed to include the investigation of structural response at different weight configurations and the maximum weapon-delivery speed of the aircraft and the structural response due to a side gust impingement. These changes provided the necesary information to evaluate refinements in the dynamic analysis.

Chapter 2
PROCEDURE

2.1 OPERATIONS

After the requirement for participation of the F-89 in Operation Plumbbob had been established, Northrop Aircraft, Incorporated (NAI), was contracted to assist the Wright Air Development Center (WADC) in planning and conducting the tests.

Since usable instrumentation had been previously installed for other flight-test operation, F-89D Serial No. 51-411 was selected as the test vehicle. After minor additions had been made to the original instrumentation, the aircraft was calibrated by NAI.

Upon completion of the calibration, the F-89D was ferried to Edwards Air Force Base, California, to begin a flight-test shakedown of all instrumentation. These shakedown flights were continued at Indian Springs Air Force Base, Nevada (ISAFB), after the F-89D arrived there on 12 April 1957. Approximately 30 practice missions were made during this phase to develop air-crew proficiency and to provide an in-flight calibration of certain instrumentation.

At the NTS, the calibration, maintenance, and operation of the instrumentation and its associated equipment plus the reduction and correlation of data were performed by the contractor. The development of positions and positioning methods were accomplished jointly by WADC and contractor personnel. The test aircraft was flown and maintained during the tests by the WADC Directorate of Flight and All Weather Testing.

The major operational problems at the test site were verifying the choice of shot participations and devising suitable aircraft positions and flight patterns for changing conditions during the operation.

2.1.1 Shot Participation. In making a choice of shot participations, it was necessary to evaluate various positioning factors as related to the limiting criteria set forth in Chapter 1 and to select the desired gust loading effect which would best satisfy the objectives of this project. The choice of shot participations based on the criteria of Reference 1 is presented in Table 2.1. These criteria were established by studies such as the one presented in Reference 2.

For Shots Boltzmann and Franklin, the aircraft was positioned to be directly over ground zero at the time of shock arrival. For Shots Wilson, Priscilla, Diablo, Kepler, Owens, Shasta, and Smoky, the aircraft was positioned to be approaching ground zero at the time of shock arrival. For Shots Hood and Franklin Prime, the aircraft was positioned to be tail on to ground zero at time of shock arrival. For Shots Stokes and Doppler, the aircraft was positioned to be side on to ground zero at time of shock arrival.

Since Shot John was an actual delivery of the MB-1 weapon, the Project 5.5 F-89D was positioned to fly formation with the F-89J delivery aircraft. At time of launch, the Project 5.5 aircraft and the delivery aircraft banked in opposite directions, and each performed a typical escape maneuver as determined by the F-89J capability study.

2.1.2 Aircraft Positioning. After determination of the desired positions for each participation, the problem of accurately positioning the aircraft remained to be solved.

In addition, a permanent time history of the position was required. Experience in Operation Redwing proved that the MSQ-1A Radar in conjunction with the Radar Data Recorder was a satisfactory positioning system (Reference 10). Consequently, this system was chosen to position the F-89D during Operation Plumbbob.

The MSQ-1A Radar system positioned the aircraft by the pilot-controller method, wherein the flight path was presented on a plotting board and compared with a preplotted track. Necessary corrections were then determined by the controller and were verbally transmitted to the pilot. The azimuth, elevation, and slant-range information were relayed from the radar set to the Radar Data Recorder. After the participation, the recorded track was reduced to a plot of the aircraft position against time.

For each event the test aircraft took off from ISAFB, climbed to its test altitude, and entered a racetrack pattern under MSQ control. One basic pattern was used for all participations. The racetrack pattern consisted of two 4-minute legs and two 2-minute turns and was planned so that the final inbound leg began approximately 50

TABLE 2.1 SHOT PARTICIPATION AND PREDICTED INPUT

N, Negligible

Shot	Aircraft Weight Configuration *	Critical Station †	Critical Load ‡	Limit Load	Overpressure	Temperature Rise	Nuclear Radiation
				pct	psi	F	rem
Boltzmann	2	WS 290	T-BM	82	0.35	20	N
Franklin	2	WS 267	V-T	80	0.23	N	N
Wilson	2	WS 267	V-T	80	0.44	N	N
Priscilla	2	WS 267	BM-T	80	0.51	N	N
Hood	2	WS 267	BM-T	86	0.32	100	N
Diablo	3	WS 267	BM-T	80	0.40	N	N
John	2	WS 50	V-T	100	0.38	N	6.18
Kepler	2A	WS 267	BM-T	84	0.36	N	N
Owens	2A	WS 267	BM-T	83	0.39	N	N
Stokes	2A	WS 267	BM-T	95	0.60	100	2.40
Shasta	3	WS 290	V-T	86	0.58	N	4.98
Doppler	2	FS 535	SBM-VBM	85	0.50	32	N
Franklin Prime	3	WS 205	T-V	76	0.47	40	4.95
Smoky	2	WS 267	BM-T	83	0.38	N	N

* 2: Symmetrical (no fuel in outboard wing or tip tanks); 2A: Unsymmetrical (same as 2 with an MB-1 Weapon mounted on the left pylon); 3: Symmetrical (same as 2 with 900 pounds of rockets installed in each tip pod).

† WS: Wing Station; FS: Fuselage Station.

‡ BM: Bending Moment; V: Shear; T: Torsion; SBM: Side Bending Moment; VBM: Vertical Bending Moment.

nautical miles from the time zero position. This type of pattern, illustrated in Figure 2.1, was used to establish the precise timing which was required by Project 5.5 throughout the duration of the test.

2.2 INSTRUMENTATION

Instrumentation was installed in the test aircraft to provide flight data necessary to substantiate the method of analysis used in the F-89J Weapons System Capability Study. This instrumentation included strain-gage installations at several wing, fuselage, and horizontal-tail stations for determination of structural loads; extensive accelerometer installations in the wing, fuselage, horizontal tail, and vertical tail for correlation of structural response; overpressure transducer installations for determination of blast and gust correlations with the structural response; and thermocouple installations at several locations for thermal response.

The location on the aircraft of pressure transducers, accelerometers, strain gages, and thermocouples is shown in Figure 2.2. Instrument types and characteristics (man-

ufacturer's specifications) are summarized in Table 2.2 and Figures 2.3 through 2.6. Detailed information is presented in Reference 11.

2.2.1 Recording Equipment. A central recording system was installed in the nose section of the aircraft instead of the fuel tank and fire-control radar system. The primary test data was recorded on three oscillographs which had a total recording capacity of 90 data channels. Test information of a supplementary nature was recorded by photographing a 24-instrument photopanel with a 35-mm camera. Correlation between recording devices was obtained with an electrical pulse from an intervalometer which actuated a counter on the 35-mm camera and a galvanometer in each oscillograph.

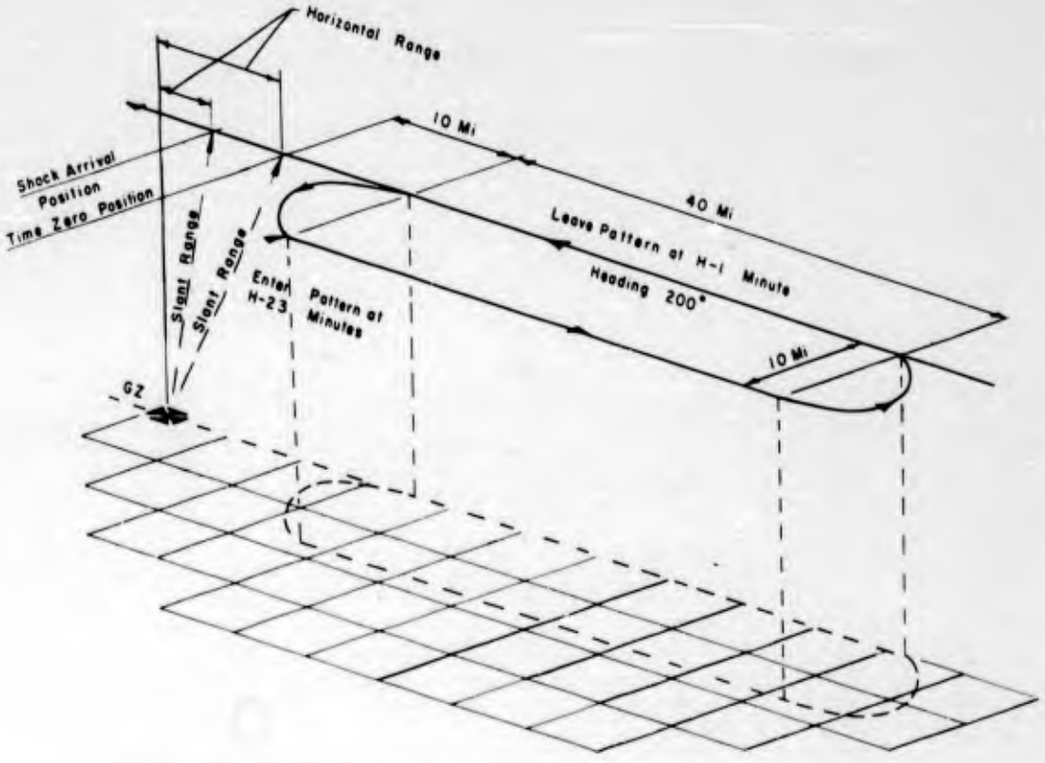

Figure 2.1 Typical MSQ flight pattern for the F-89D. One complete 12-minute pattern was required to position the aircraft.

The time-zero position was recorded on the oscillograph recordings as that point where the radiometer trace first deviated from the ambient during the thermal phase.

2.2.2 Gust Input. Fourteen pressure transducers were installed in the tip pod, fuselage, and vertical tail of the test aircraft to measure the magnitude of the overpressure associated with the passage of the shock wave. Each transducer measured the differential pressure between the static orifice and a container vented to ambient pressure through a line which contained a solenoid-actuated valve. The solenoid valve was actuated just prior to time zero in order to capture a sample of ambient pressure in the container which served as a reference pressure for comparison with the gust overpressure.

The transducers were located in a manner to enable determination of shock-front direction and velocity. In addition, free-stream vane indicators were installed on a

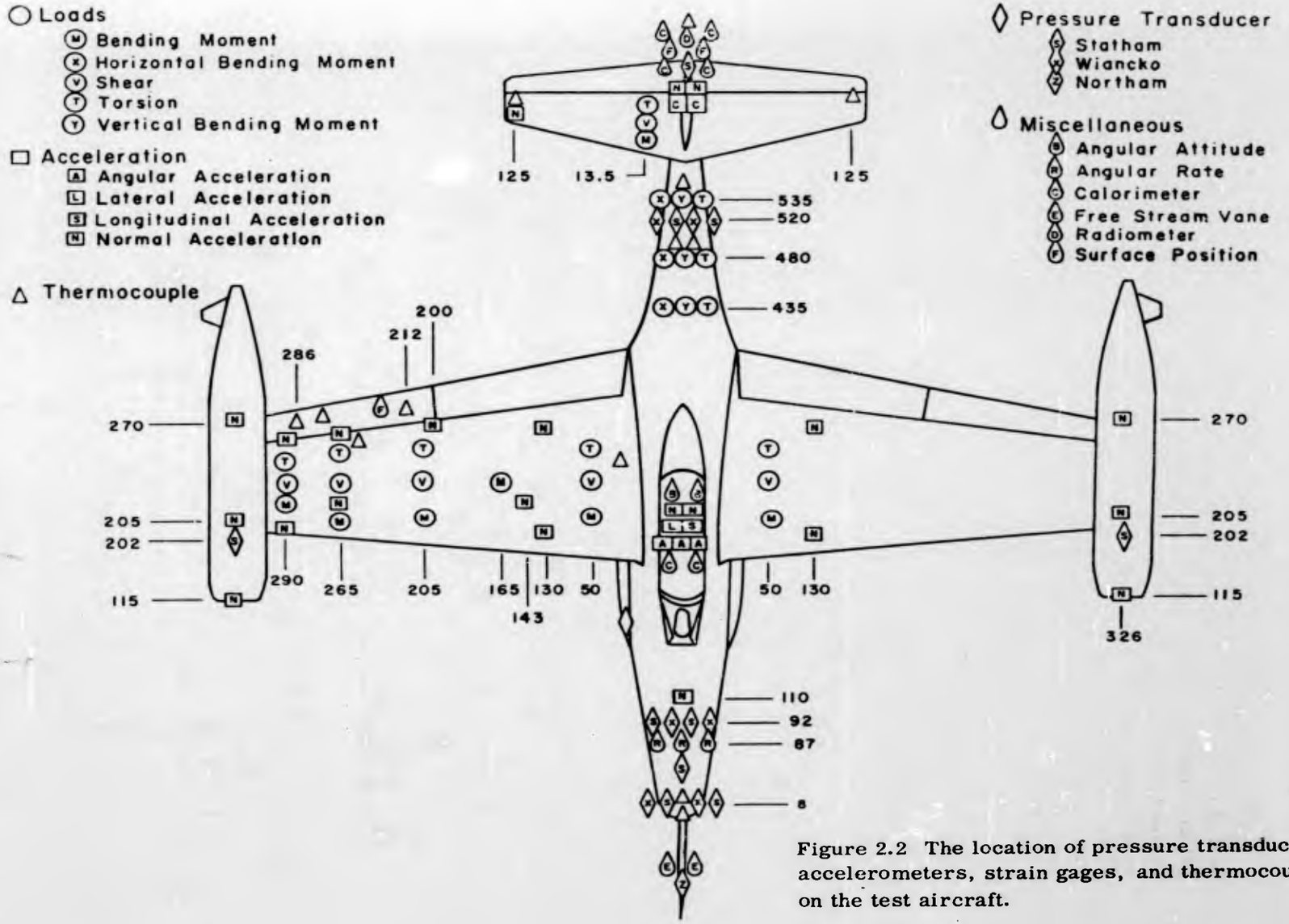

Figure 2.2 The location of pressure transducers, accelerometers, strain gages, and thermocouples on the test aircraft.

boom ahead of the aircraft. These indicators were used to evaluate the gust inputs by sensing changes in angle of attack and sideslip.

2.2.3 Gust Response. Twenty-six linear accelerometers sensed the dynamic response of the aircraft as it was subjected to overpressure and gust inputs: 22 at locations in the tip pod, wing, fuselage, and horizontal stabilizer to measure accelerations normal to the aircraft flight path; 3 in the fuselage and vertical stabilizer to sense lateral acceleration; and 1 in the fuselage to measure longitudinal acceleration. In addition, during those tests in which a dummy MB-1 weapon was attached to the left-hand

TABLE 2.2 MANUFACTURER'S INSTRUMENT SPECIFICATIONS

GALVANOMETERS:								
Make	CEC	CEC						
Model	7-315	7-318						
Undamped Natural Frequency, cps	100	150						
Flat (±5 pct) Frequency Range, cps	0-60	0-90						
External Damping Resistance, ohms	350	180						
Sensitivity at 11.5-inch Optical Arm:								
Undamped dc, μa/in	12.2	30.6						
System voltage sensitivity, mv/in	4.67	6.29						
LINEAR ACCELEROMETERS:								
Make	Statham	Statham	Statham	Statham	Statham	Statham	Wiancko	Wiancko
Model	C-2.5-120	C-5-120	C-10-120	C-15-120	C-20-120	C-25-120	AC-1002	A-1002
Acceleration Range, g	±2.5	±5	±10	±15	±20	±25	±3	±6
Rated input Voltage (ac-dc), volts	11	11	11	11	11	11	20	20
Output Voltage, Full Scale, mv	20	23	24	25	25	24	192	192
Temperature Limits, degrees Fahrenheit	−40 to + 200	−40 to + 200	−40 to + 200	−40 to + 200	−40 to + 200	−40 to + 200	Temp Comp	Temp Comp
Natural Frequency, cps	50	75	110	160	180	200	58	58
ANGULAR ACCELEROMETERS:								
Make	Statham	Statham	Statham					
Model	AA-1.5-300	AA-3-300	AA-5-300					
Acceleration Range, radians/sec^2	1.5	3	5					
Rated Input Voltage (ac-dc), volts	10	10	10					
Output Voltage, Full Scale, mv	20	20	20					
Temperature Limits, degrees Fahrenheit	−40 to + 200	−40 to + 200	−40 to + 200					
Natural Frequency, cps	4	7	10					
RATE GYRO:								
Make	Doelcam							
Model	K-75							
Range, degrees/sec	±30							
Full Scale Output, volts	1.04							
Sensitivity, volts/degree-sec	0.035							
Damping Ratio	0.63							
Undamped Natural Frequency, cps	27							
ATTITUDE GYRO:								
Make	Kearfott							
Model	T2105							
Repeatability to Established Vertical	To within a cone of half angle equal to 5 minutes of arc							
Free Drift Rate in 5 min of Time:								
At Room Temperature, degrees maximum	2							
At −54C and +71C, degrees maximum	2½							
Erection Rate:								
At Room Temperature, degrees minimum	5 ± 1							
At −54C and +71C, degrees minimum	5 ± 3							
Temperature Limits, C	−54 to + 71							
PRESSURE TRANSDUCERS:								
Make	Northam	Statham	Wiancko*					
Model	DP-7	P96-5D-120	P2-1101					
Pressure Range, psi	±5	±5	±5					
Full Scale Sensitivity, mv	40/volt	approx 25	180/volt					
Excitation, volts	10	6	10					

* Integral heater installed.

launcher, linear accelerometers were installed on the launcher rail to sense normal and longitudinal accelerations. All linear accelerometers except those in the wing and tip pods were filtered. For frequency-response characteristics of filtered accelerometers, refer to Figure 2.6.

Three angular accelerometers were installed to measure pitch, roll, and yaw accelerations about the aircraft center of gravity. Rate and attitude gyros were installed to sense the aircraft attitude changes.

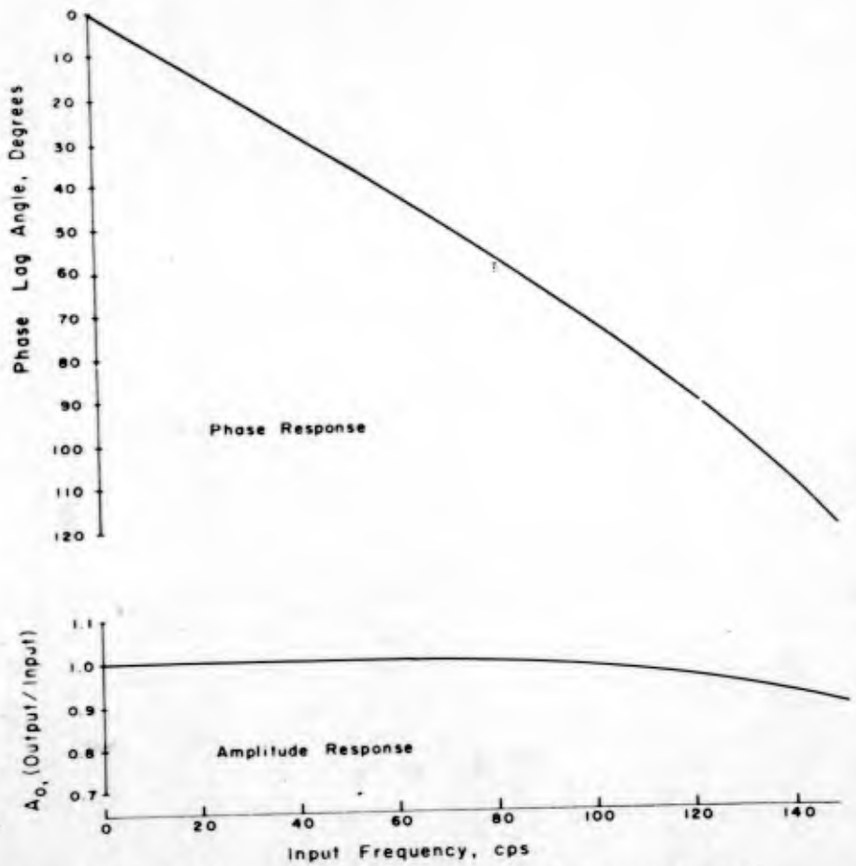

Figure 2.3 Typical dynamic response characteristics of overpressure sensing systems, Statham pressure transducer.

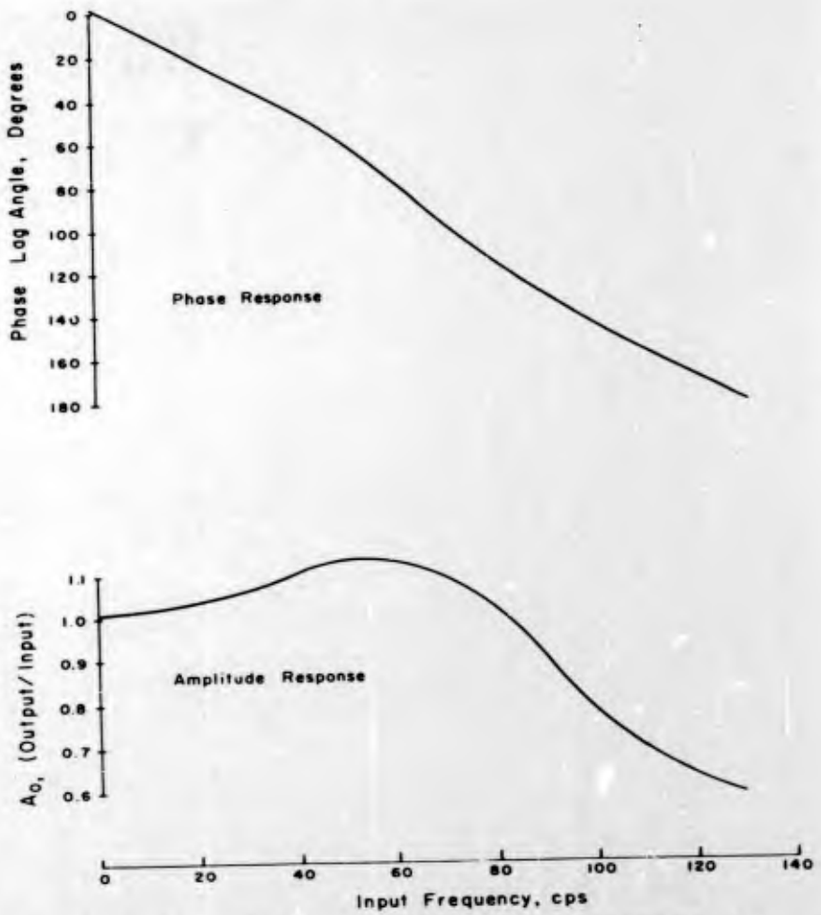

Figure 2.4 Typical dynamic response characteristics of overpressure sensing systems, Wiancko pressure transducer.

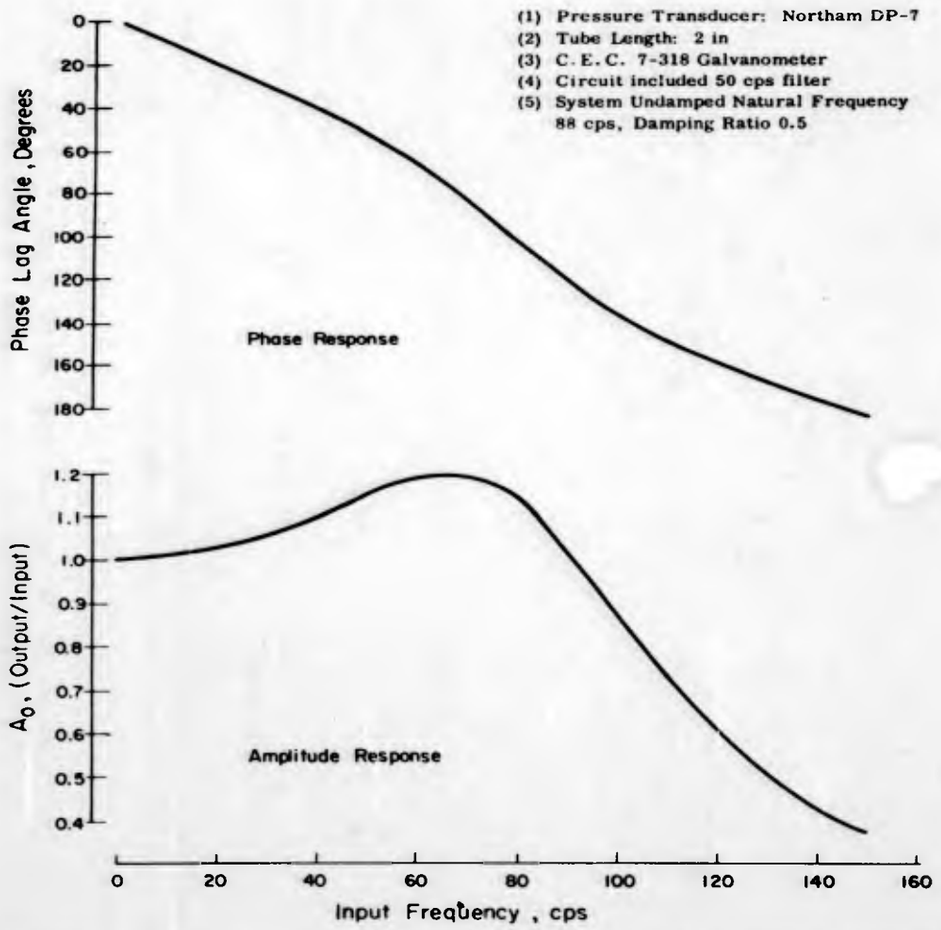

Figure 2.5 Typical response characteristics of overpressure sensing systems, Nose Boom– Northam Pressure Transducer.

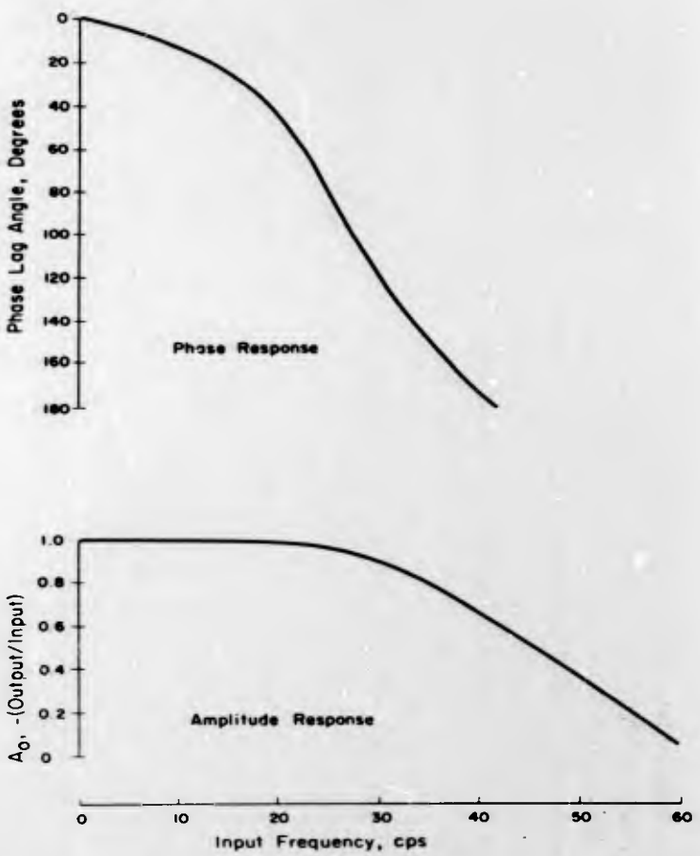

Figure 2.6 Typical dynamic response characteristics of all filtered accelerometer channels.

In order to measure the flight loads imposed on the primary structure by the gust inputs, strain-gage bridges were installed as follows: at Right-Wing Stations 50.0, 165.0, 205.0, 267.0, and 290.0 and Left-Wing Station 50.0, as shown in Figure 2.7; at Fuselage Stations 435.0, 480.0 and 535.0 as shown in Figure 2.8; and at Right-Stabilizer Station 13.5 as shown in Figure 2.9.

An N-9 camera was installed to obtain wing deflections; however, the data recorded was not satisfactory for correlation with strain gage data.

2.2.4 Thermal Input. The thermal energy received by the aircraft was measured with instrumentation furnished by the U. S. Naval Radiological Defense Laboratory (NRDL).

Two calorimeter, one radiometer, and two N-9 cameras were packaged together in an adjustable assembly. Prior to each event, this assembly was installed in either the

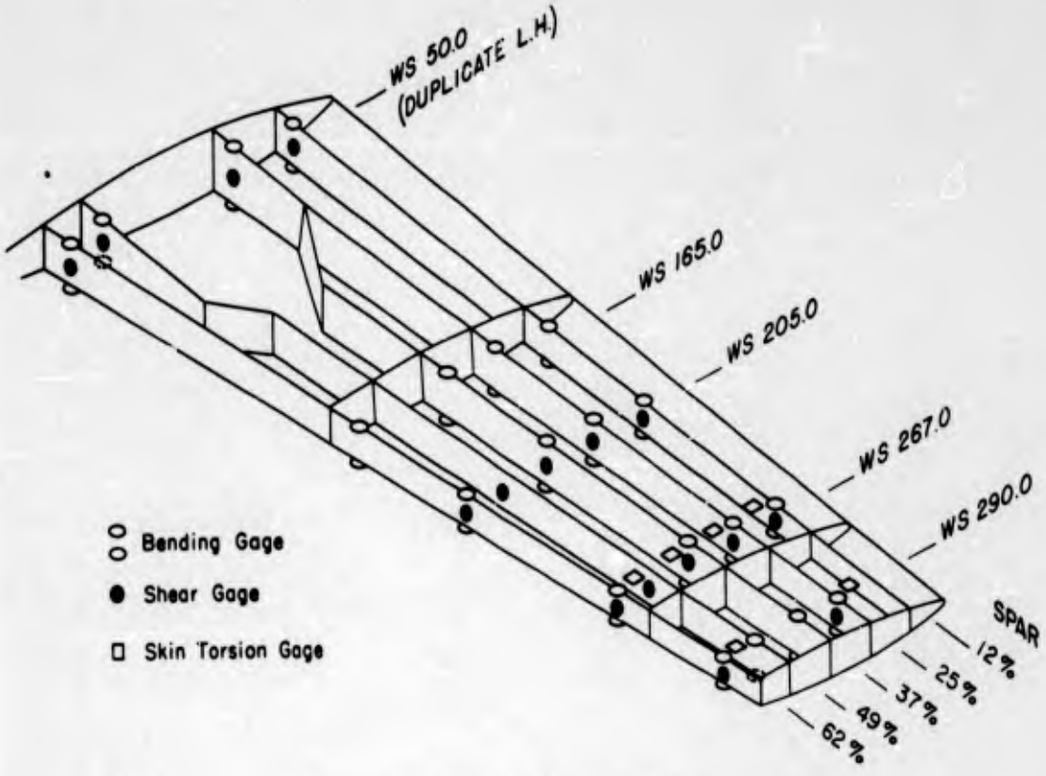

Figure 2.7 Wing strain-gage locations.

aircraft tail-cone fairing or in the forward section of either wing tip pod, depending upon the expected position of the aircraft relative to ground zero. The camera records were used to determine the actual orientation of the calorimeters and radiometers with respect to the point of detonation.

Two calorimeters were installed in the crew compartment to measure the scattered radiant exposure that entered the cockpit, and two calorimeters were installed in the tail cone to measure the scattered radiant exposure from below the aircraft normal to the flight path.

2.2.5 Thermal Response. Thirteen washer-type, copper-constantan thermocouples were installed on critical areas of the rudder, both elevators, right aileron, both wings,

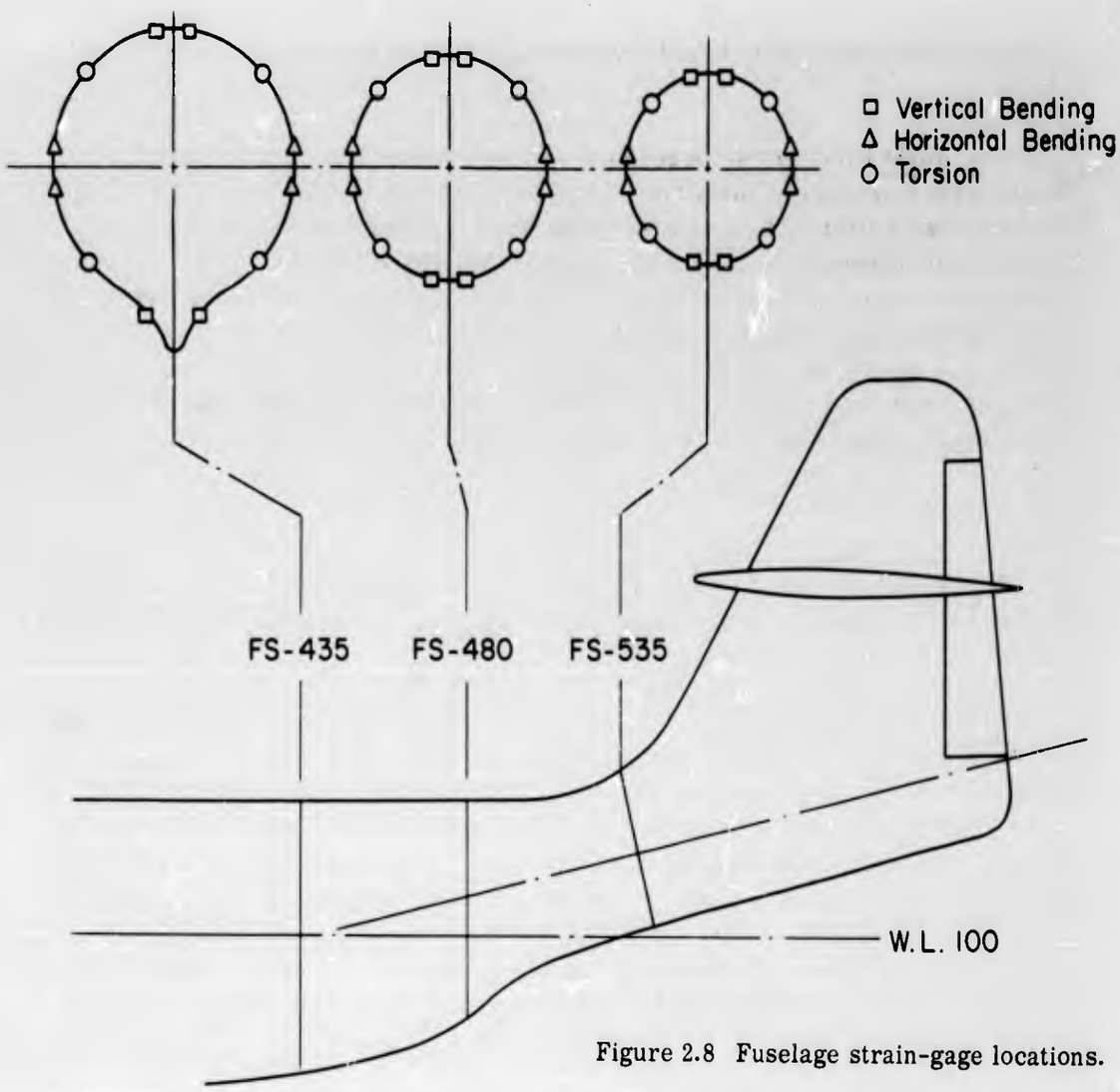

Figure 2.8 Fuselage strain-gage locations.

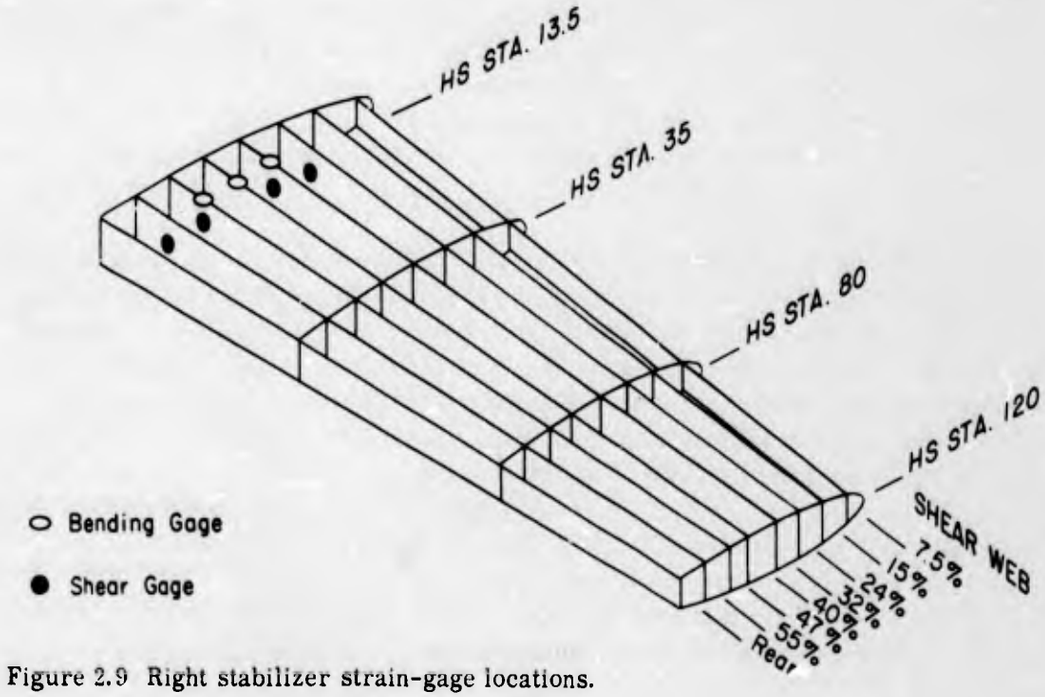

Figure 2.9 Right stabilizer strain-gage locations.

fuselage, and radome surface. All thermocouples were referenced to an ice bath at 32 F.

2.2.6 Flight Parameters. A sensitive airspeed and altitude system was installed with the pressure source located on a boom 8 feet forward of the nose section. Supplementary information such as ambient temperature, compass heading, engine speed, exhaust-gas temperature, and time were measured with standard flight-test instruments and were recorded on the photo panel. The angular positions of the F-89D control surfaces were measured with strain-gage, bending-beam instrumentation.

2.2.7 Positioning Equipment. An APW-11A transponder unit and associated equipment were installed for use with the MSQ-1A radar.

2.3 CALIBRATION

The primary calibration procedures used for Project 5.5 are listed in this section. Detailed information on the calibration techniques used for all aircraft instrumentation is listed in Reference 11.

2.3.1 Pressure Transducers. Static calibrations were conducted on each transducer before and after its installation in the aircraft, and at frequent intervals during the test program. The initial calibration was conducted to verify the linear response of the instrumentation. Subsequent calibrations consisted of checks of the transducer output. These were conducted by applying known pressures in increments throughout the range of the instrument while the transducer output was being recorded in the test recording system. A frequency-response analysis of the pressure system was conducted by applying a step pressure increment at the static orifice. The system frequency response was then calculated from the oscillograph record by using a Fourier integral method (Reference 12).

2.3.2 Accelerometers and Gyros. The accelerometers were calibrated in the laboratory before being installed in the aircraft. This calibration consisted of a complete linearity check through the range of the instrument. A centrifuge was used to supply the required accelerations needed for this test.

Prior to and at frequent intervals during the test program, a calibration of each transducer was conducted. For this test a pendulum and a tilt table were used to establish ±5.0-g, ±1.0-g, and 0.0-g forces while the transducer output was being recorded on the test recording system.

The calibration procedures for the rate and attitude gyros was similar to those used for the accelerometers. Prior to installation of the instrument, a laboratory calibration was conducted to verify the linearity of each response. The rate gyros were then calibrated by mounting them on a precision rate table and recording the instrument response for various table speeds. The attitude gyros were calibrated by mounting them on a tilt table and recording the instrument output through the test recording system for various angular positions of the table.

2.3.3 Strain Gage Bridges. The strain gage bridges were calibrated by applying known loads at points on the instrumented structure (Reference 13). The individual bridge response to these loads was recorded. Those bridges having complementary characteristics were mathematically combined into an equation which could be used to

compute bending moment, shear, and torsion as a linear function of the combined bridge response, regardless of the point of load application. At frequent intervals during the program, check calibrations were conducted to reveal any changes in gage sensitivity.

2.3.4 Thermocouples. The thermocouples were calibrated by applying incremental mv inputs through the thermocouple and recording the instrument output on the test recording system.

2.3.5 Calorimeters and Radiometers. The basic instrument calibrations were provided by NRDL. Prior to each test, mv/in calibrations were conducted using an accurate mv source.

2.3.6 Supplementary Instrumentation. The instruments installed in the photo panel were calibrated using standard flight test procedures. No calibration of the airspeed system was necessary, since the position errors for this system had been well established on previous test programs. The control-surface position indicators were calibrated by moving the control surfaces through the range of use and recording the output of the instrument on the aircraft recording system.

Chapter 3
RESULTS and DISCUSSION

The data obtained from the participation of the F-89D in Operation Plumbbob represents the primary results of Project 5.5. The complete data, in the form of motion-picture film and time history plots, are presented in Reference 14. Final results in the form of peak readings are presented here to fulfill the requirements of this report.

General flight data, meteorological data, and peak readings of principal input and response measurements are presented in Tables 3.1 through 3.8. All predicted input and response values shown in the tables are based on the actual test aircraft position, final postshot yield, and unit-response data derived from the test results. Sample time histories of representative inputs and responses are shown in Figures 3.1 through 3.3. The method of reading peak load and corresponding torsion from the time histories is presented in Figure 3.1. The allowable wing-load envelopes used to determine the critical nature of these load combinations are shown in Figures 3.4 and 3.5 with a sample series of predicted and recommended loads plotted on the figures. General observations for each event are presented in the succeeding paragraphs.

3.1 SHOT BOLTZMANN

The aircraft was positioned to obtain 82 percent of design-limit load in the wing tip area, based on analytical dynamic loads. The desired position was at an altitude of 20,000 feet and directly over ground zero, providing a gust (dynamic-pressure wave) impingement angle of 90 degrees. Because of the normal impingement angle, both gust loads and diffractive loads were included in determining the percent of design limit load. The symmetrical weight configuration (2) as described in Table 2.1 was used for this test with a desired aircraft speed of Mach 0.775.

All aircraft instrumentation functioned properly. However, there was a delay in the timing signal transmitted to the positioning controller resulting in an aircraft position slightly short of ground zero at shock arrival time. The aircraft was subjected to two shock waves because of the position inside the triple point path.

The recorded wing loads showed considerable disagreement with the analytical loads, using preshot prediction methods, and postshot position and weapon effects. The critical analytical-load combination occurred at Wing Station 290; however, the critical measured value occurred at Wing Station 267 and consisted of peak positive bending moment with a small corresponding negative torsion. This measured load combination was equal to 84 percent of design limit load, while the magnitude of the predicted load combination at Wing Station 267 was only 43 percent. Thus, not only did the critical station differ from anticipated, but the measured load at Wing Station 267 was 41 percent more critical than predicted. All the measured bending moments and shear loads spanwise of the wing were of higher magnitude than had been predicted. A comparison of analytical and measured peak combination loads at each instrumented wing station is presented in Table 3.9.

A further complication developed about an adjustment factor that had been applied to the calibration constants in the equation derived to obtain the shear load at Wing

TABLE 3.1 AIRCRAFT POSITION AT TIME ZERO

Shot	Altitude True		Horizontal Range		Offset, + = Right − = Left		Slant Range		Wing Angle of Attack, Nose up, Degrees from Horizontal	Angle Between Horizontal Receiver and Line to Burst	
	Desired	Measured	Desired	Measured	Desired	Measured	Desired	Measured		Predicted	Measured
	ft	ft	ft	ft	ft	ft	ft	ft	deg	deg	deg
Boltzmann	20,000	20,400	−10,700	−11,460	0	200	18,700	19,430	1.07	54.7	53.7
Franklin	19,000	18,800	−10,200	−10,100	0	0	17,900	17,670	0.0	55.0	55.2
Wilson	17,000	16,880	−28,750	−34,940	0	50	31,300	36,990	0.95	23.0	19.1
Priscilla	16,000	15,870	−34,600	−35,440	0	550	36,700	37,450	0.92	19.4	18.9
Hood	26,000	26,000	+3,600	+2,900	0	530	20,600	20,320	1.43	79.6	81.8
Diablo	19,000	19,070	−31,300	−31,730	0	0	34,300	34,720	1.43	24.1	24.0
John	18,500	19,430	−10,740	−11,000	+130	300	10,740	11,010	1.13	—	—
Kepler	17,500	17,690	−31,400	−32,670	0	380	33,870	35,120	2.20	22.6	21.5
Owens	16,000	16,140	−30,700	−31,030	0	300	32,710	33,070	0.99	20.2	20.2
Stokes	15,000	15,000	−850	−680	−6,000	−6,100	11,100	11,160	0.90	21.6	21.6
Shasta	15,000	15,170	−22,500	−23,050	0	250	24,660	25,240	0.83	24.2	24.0
Doppler	12,000	12,300	−3,120	−3,820	−11,000	−10,970	13,060	13,370	0.93	28.9	29.7
Franklin Prime	13,200	13,260	+204	+380	0	0	8,270	8,340	0.80	88.6	87.4
Smoky	20,000	20,100	−48,520	−48,820	0	750	50,730	51,050	1.10	17.0	17.0

TABLE 3.2 AIRCRAFT FLIGHT CONDITIONS AT TIME ZERO

Shot	Temperature *	True Air Speed		Mach Number		Gross Weight, Desired and Measured	Center of Gravity, Desired and Measured
		Desired	Measured	Desired	Measured		
	C	ft/sec	ft/sec			lb	pct of MAC
Boltzmann	−19.0	815	810	0.775	0.773	33,600	23.80
Franklin	−6.0	833	824	0.775	0.767	33,600	23.80
Wilson	+1.0	834	832	0.765	0.764	33,600	23.80
Priscilla	+4.0	827	821	0.755	0.751	33,600	23.80
Hood	−19.0	794	798	0.755	0.761	33,600	23.80
Diablo	−5.0	815	813	0.755	0.755	34,120	22.10
John	−10.0	808	810	0.760	0.759	33,600	23.80
Kepler	−4.0	815	853	0.755	0.792	34,920	22.07
Owens	−4.0	815	828	0.755	0.767	34,920	22.07
Stokes	−1.2	819	824	0.755	0.761	34,920	22.07
Shasta	+3.5	827	833	0.755	0.762	34,120	22.10
Doppler	+7.0	831	824	0.755	0.749	33,600	23.80
Franklin Prime	+3.5	827	823	0.755	0.753	34,920	22.07
Smoky	−16.0	898	888	0.850	0.843	33,600	23.80

* Ambient temperature recorded by the aircraft.

TABLE 3.3 AIRCRAFT POSITION AT SHOCK ARRIVAL

Shot	Altitude, True		Horizontal Range		Offset, + = Right, − = Left		Slant Range		Wing Angle of Attack, Nose up, Degrees from Horizontal	Angle Between Horizontal Receiver	
	Desired	Measured	Desired	Measured	Desired	Measured	Desired	Measured		Predicted	Measured
	ft	ft	ft	ft	ft	ft	ft	ft	deg	deg	deg
Boltzmann	20,000	20,560	0	−1,370	0	+100	15,300	15,720	1.07	90.0	85.0
Franklin	19,000	18,830	0	+150	0	−50	14,700	14,530	1.13	90.0	90.0
Wilson	17,000	16,820	−15,500	−19,070	0	+850	19,770	22,600	0.95	38.3	32.3
Priscilla	16,000	15,820	−19,850	−20,230	0	+640	23,310	23,550	0.92	31.5	30.8
Hood	26,000	26,160	+22,600	+23,060	0	+770	30,360	30,840	1.43	42.0	41.5
Diablo	19,000	19,160	−17,100	−17,290	0	+260	22,120	22,370	1.13	39.3	39.4
John	18,500	19,430	−6,680	−6,240	+1,750	+2,570	6,900	6,760	2.20	—	*
Kepler	17,500	17,900	−17,220	−17,440	0	+500	21,400	21,810	0.99	36.3	36.8
Owens	16,000	16,070	−17,200	−17,330	0	+520	20,580	20,720	0.90	33.2	33.2
Stokes	15,000	15,000	+7,500	+7,600	−6,000	−6,100	13,380	13,500	0.83	44.2	43.6
Shasta	15,000	15,290	−12,500	−12,750	0	+200	16,080	16,460	0.93	39.0	39.2
Doppler	12,000	12,270	+6,000	+5,350	−11,000	−10,840	14,030	13,760	—	26.9	28.6
Franklin Prime	13,200	13,290	+7,440	+7,400	0	+80	11,100	11,160	0.80	48.2	48.5
Smoky	20,000	20,100	−26,330	−26,510	0	+750	30,120	30,430	1.10	29.3	29.4

* Co-altitude burst.

TABLE 3.4 AIRCRAFT FLIGHT CONDITIONS AT SHOCK ARRIVAL

Shot	Temperature *	True Air Speed		Mach Number		Gross Weight, Desired and Measured	Center of Gravity, Desired and Measured
		Desired	Measured	Desired	Measured		
	C	ft/sec	ft/sec			lb	pct of MAC
Boltzmann	−19.0	813	807	0.775	0.768	33,600	23.80
Franklin	−6.0	834	824	0.775	0.766	33,600	23.80
Wilson	+1.0	834	833	0.765	0.764	33,600	23.80
Priscilla	+4.0	815	824	0.755	0.752	33,600	23.80
Hood	−19.0	793	796	0.755	0.758	33,600	23.80
Diablo	−5.0	814	809	0.755	0.750	34,120	22.10
John	−10.0	812	801	0.760	0.750	33,600	23.80
Kepler	−4.0	815	819	0.755	0.758	34,920	22.07
Owens	−4.0	815	847	0.755	0.784	34,920	22.07
Stokes	−1.0	820	824	0.755	0.758	34,920	22.07
Shasta	+3.5	827	832	0.755	0.760	34,120	22.10
Doppler	+7.0	832	828	0.755	0.751	33,600	23.80
Franklin Prime	+3.5	827	822	0.755	0.751	34,920	22.07
Smoky	−16.0	897	882	0.850	0.835	33,600	23.80

* Ambient temperature recorded by the aircraft.

TABLE 3.5 THERMAL AND NUCLEAR INPUTS

N: negligible

Shot	Total Radiant Exposure, Direct		Peak Irradiance	Time of Peak Irradiance	Nuclear Radiation		
	Predicted*	Measured	Measured	Measured	Predicted*	Received Pilot Cockpit Location	Received Observer Cockpit Location
	cal/cm^2	cal/cm^2	(cal)/cm^2/sec	sec	rem	rem	rem
Boltzmann	1.21	1.08†	2.10	0.16	N	0	0.020
Franklin	Recorded Data Too Low For Accuracy						
Wilson	N	0.20	0.60	0.13	N	0	0
Priscilla	N	0.71	1.47	0.23	N	0	0
Hood	6.16‡	6.00‡	6.82	0.26	N	0	0.055
Diablo	N	0.25	0.53	0.22	N	0	0
John	N	0.36	3.92	0.06	3.74	3.55	2.44
Kepler	N	0.05	0	—	N	0	0
Owens	N	0.27	0.85	0.10	N	0	0
Stokes	5.23	5.35†	11.19	0.16	1.39	0.855	0.850
Shasta	N	0.27	0.56	0.20	3.44	1.16	1.16
Doppler	2.24	1.96†	6.47	0.13	N	0.10	0.10
Franklin Prime	2.84‡	2.86‡	10.57	0.09	3.70	2.44	2.05
Smoky	N	0.37	0.52	0.24	N	0	0

* Predictions based on Final positions and yields, Table 1.1.

† Measured normal to direct rays.

‡ Measured parallel to ground.

TABLE 3.6 OVERPRESSURE INPUTS

Shot	Shock Arrival Time, First Shock Wave		Overpressure, First Shock Wave		Shock Arrival Time, Second Shock Wave		Overpressure, Second Shock Wave	
	Predicted*	Measured	Predicted*	Measured	Predicted*	Measured	Predicted*	Measured
	sec	sec	psi	psi	sec	sec	psi	psi
Boltzmann	12.84	12.95	0.306	0.321	13.89	14.86	0.276	0.246
Franklin	Recorded Data Too Low for Accuracy							
Wilson	18.83	18.96	0.267	0.276	—	—	—	—
Priscilla	18.78	18.72	0.457	0.464	—	—	—	—
Hood	25.02	26.03	0.252	0.224	28.51	28.72	0.217	0.080
Diablo	18.37	18.33	0.332	0.328	—	—	—	—
John	5.50	5.64	0.398	0.357	—	—	—	—
Kepler	18.21	18.23	0.273	0.274	—	—	—	—
Owens	17.23	17.00	0.295	0.287	—	—	—	—
Stokes	10.35	10.73	0.528	0.497	13.60	14.07	0.386	0.409
Shasta	12.93	12.81	0.519	0.511	—	—	—	—
Doppler	10.79	10.83	0.423	0.404	12.85	12.87	0.345	0.232
Franklin Prime	8.92	9.00	0.380	0.334	10.61	11.07	0.307	0.249
Smoky	25.53	25.12	0.313	0.298	—	—	—	—

* Predictions based on final positions and yields, Table 1.1.

TABLE 3.7 GUST RESPONSE, CRITICAL STATION

Shot	Critical Station	Type of Critical Load Combination*	Bending Moment		Shear		Corresponding Torsion Load		Percent Limit Load	
			Predicted†	Measured	Predicted†	Measured	Predicted†	Measured	Predicted†	Measured
			in-lb	in-lb	lb	lb	in-lb	in-lb	pct	pct
Boltzmann	267	BM-T	434,000	430,000	—	—	−21,000	−20,000	84	84
Franklin			Recorded Data Too Low For Accuracy							
Wilson	290	V-T	—	—	3,300	3,300	−22,420	−28,000	47	47
Priscilla	267	BM-T	347,000	358,000	—	—	−10,500	−10,000	71	72
Hood	267	BM-T	198,000	198,000	—	—	−50,000	−50,000	44	45
Diablo	290	V-T	—	—	−3,790	−3,400	−98,500	−110,000	53	50
John	50	V-T	—	—	19,700	18,300	418,000	380,000	90	87
Kepler	50	V-T	—	—	10,320	10,250	308,000	280,000	48	47
Owens	50	V-T	—	—	10,520	10,700	223,000	280,000	52	53
Stokes	290	BM-T	130,000	130,000	—	—	−90,000	−90,000	87	76
Shasta	290	BM-T	−306,000	−286,000	—	—	−216,000	−145,000	91	84
Doppler	267	BM-T	242,000	178,000	—	—	−5,800	−46,000	56	52
Franklin Prime	290	BM-T	−205,500	−228,000	—	—	−162,000	−180,000	65	73
Smoky	267	BM-T	227,000	236,000	—	—	−10,950	−20,000	57	61

* BM: Bending Moment; T: Torsion; V: Shear.
† Predictions based on final positions and yields, Table 1.1.

TABLE 3.8 METEOROLOGICAL DATA AT AIRCRAFT ALTITUDE*

Shot	Wind		Temperature	Pressure	Dew Point	Relative Humidity	Sky Conditions
	Direction	Velocity					
	deg	knots	C	mb	C	pct	
Boltzmann	155	23	−17.9	470	−20.5	82.0	4/10 Altocumulus, 1/10 Cirrus
Franklin	310	08	−9.6	508	—	—	1/10 Cirrus
Wilson	305	07	−1.7	551	—	—	Clear
Priscilla	235	07	+0.4	574	—	—	Clear
Hood	220	09	−17.8	386	—	--	Clear
Diablo	230	06	−6.4	506	−21.6	28.0	Clear
John	210	14	−10.1	500	—	—	Clear
Kepler	095	10	−7.4	529	—	—	Clear
Owens	160	21	−4.2	563	−8.1	72.6	4/10 Strata Cumulus
Stokes	180	27	−1.2	585	−15.1	34.0	Clear
Shasta	150	09	+2.0	583	−9.5	42.0	Clear
Doppler	110	12	+6.1	653	−1.0	61.0	Clear
Franklin Prime	180	19	−1.4	623	−18.8	25.0	Clear
Smoky	280	21	−15.9	478	—	—	Clear

* Data derived from official meteorological reports.

Station 267. The initial response was to assume the combination of shear and torsion at this station had exceeded design limit load, but further investigation revealed that the adjustment factor was valid only for low steady state loads. Until the investigation on the validity of this shear load was completed, after Shot Wilson and prior to Shot Priscilla, the shear and torsion combination at Wing Station 267 was the controlling factor for positioning.

The results of the Shot Boltzmann participation indicated that the analytical loads were unconservative and therefore were not safe for use in positioning. It was decided that empirical use of available test results would be applied for future positioning. To utilize the test loads they were reduced to unit values similar to the analytical unit loads. The aircraft position at shock arrival and the overpressure associated with the shock wave were obtained from the recorded data, then the gust impingement angle, total gust velocity, and effective gust velocity (KU_{e_z}) were computed by the methods defined in Chapter I. Unit test loads were then determined by dividing the maximum recorded incremental dynamic load by the effective gust velocity. After each participation, a review of all available test results was made to assure the reliability of each test point.

Although the measured wing loads did not agree with the analytical loads, the test time histories of shear and bending moment resembled the analytical time histories in shape. The discrepancy between measured loads and analytical loads was primarily in the magnitude. Recorded time histories of the wing torsion differed in magnitude and shape with the analytical magnitudes equal to or less than the measured values.

The horizontal tail and aft fuselage recorded loads were considerably less critical than the wing loads but differed from the analytical data in magnitude and shape. incident thermal energy recorded was lower than predicted, resulting in no significant temperature rise on the aircraft. The nuclear radiation dosage received by the air crew was negligible.

3.2 SHOT FRANKLIN

A position for Shot Franklin had been determined prior to the first participation based on analytical dynamic loads. The aircraft speed, weight configuration, and orientation were the same as those for Shot Boltzmann with a desired flight altitude of 15,000 feet.

The initial review of the results obtained in the Shot Boltzmann participation indicated that the existing Shot Franklin position was unsafe and could not be utilized. Using the unit test loads, based on the Boltzmann data, a new test altitude was determined to yield a predicted 80 percent design limit load. The Aircraft Mach number, weight configuration and orientation remained the same. Controlling load for this position was the positive shear-torsion combination, containing the adjustment factor, at Wing Station 267. To account for changes in altitude, the test loads were adjusted by the ratio of ambient air density and the speed of sound at the respective altitudes, in keeping with the trend displayed by the analytical loads.

All instrumentation functioned properly and the aircraft was in its planned position at both burst time and time of shock arrival. Because of the low yield of the device, the general response data obtained was too low to give reliable results. Incident thermal energy and nuclear radiation dosage were negligible.

3.3 SHOT WILSON

After the Shot Franklin participation, a thorough analysis of the Shot Boltzmann results was conducted. It was observed that the damping rate of the wing loads was

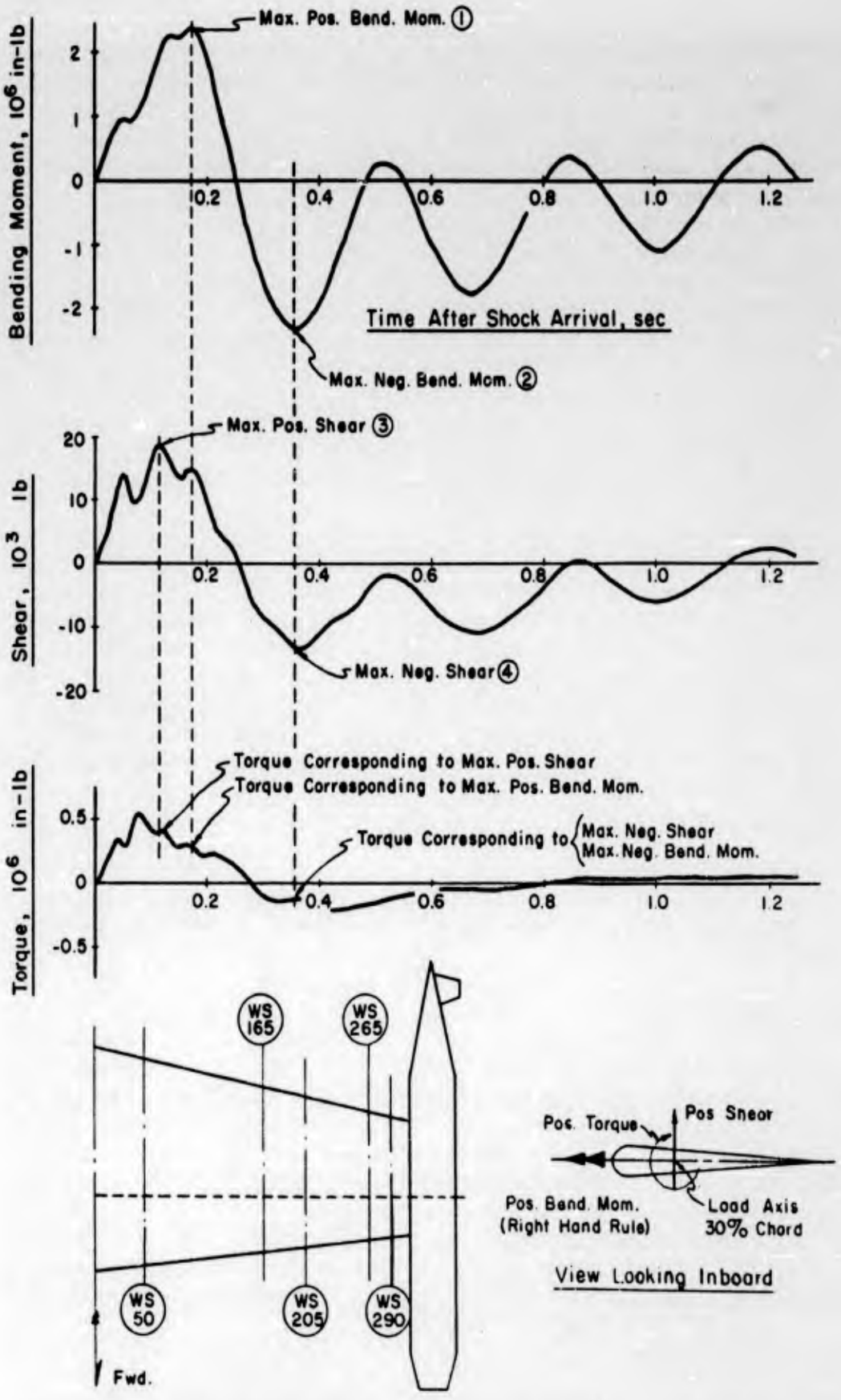

Figure 3.1 Critical load time histories for Wing Station 50. The data was obtained on Shot John.

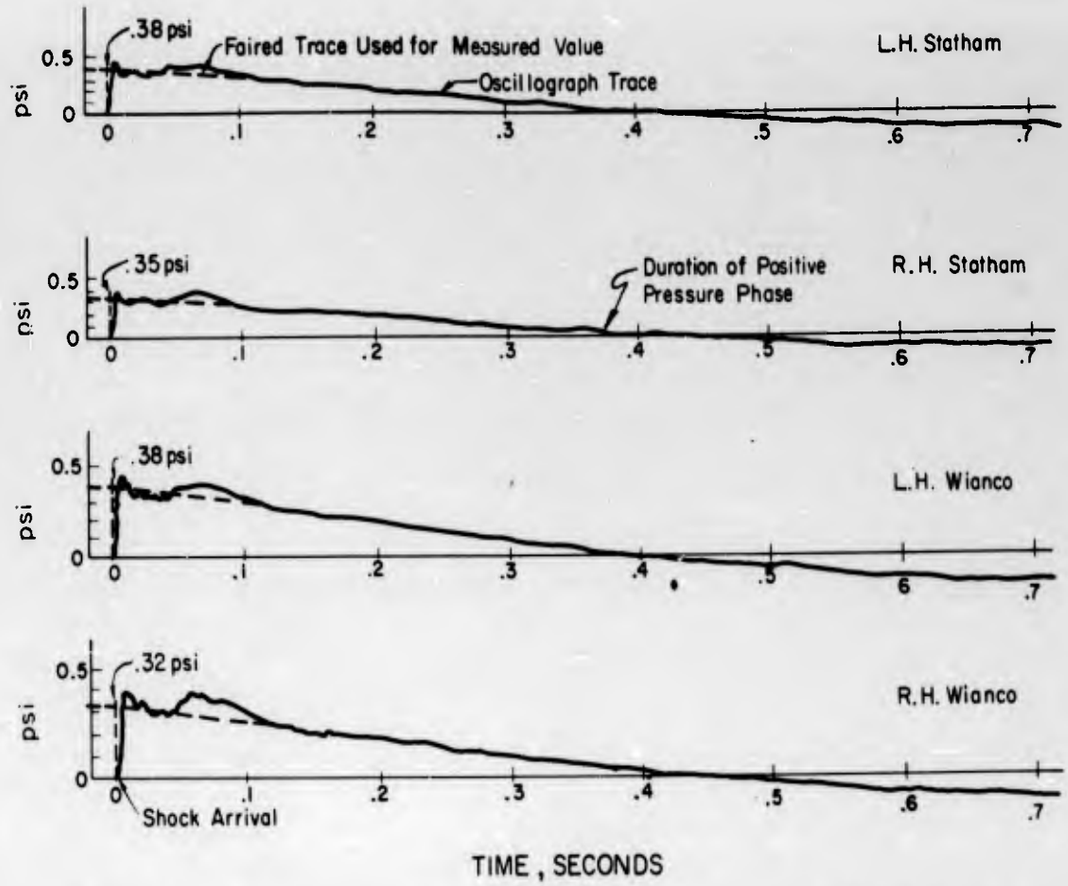

Figure 3.2 Typical overpressure-time histories, Shot John, Fuselage Station 94.

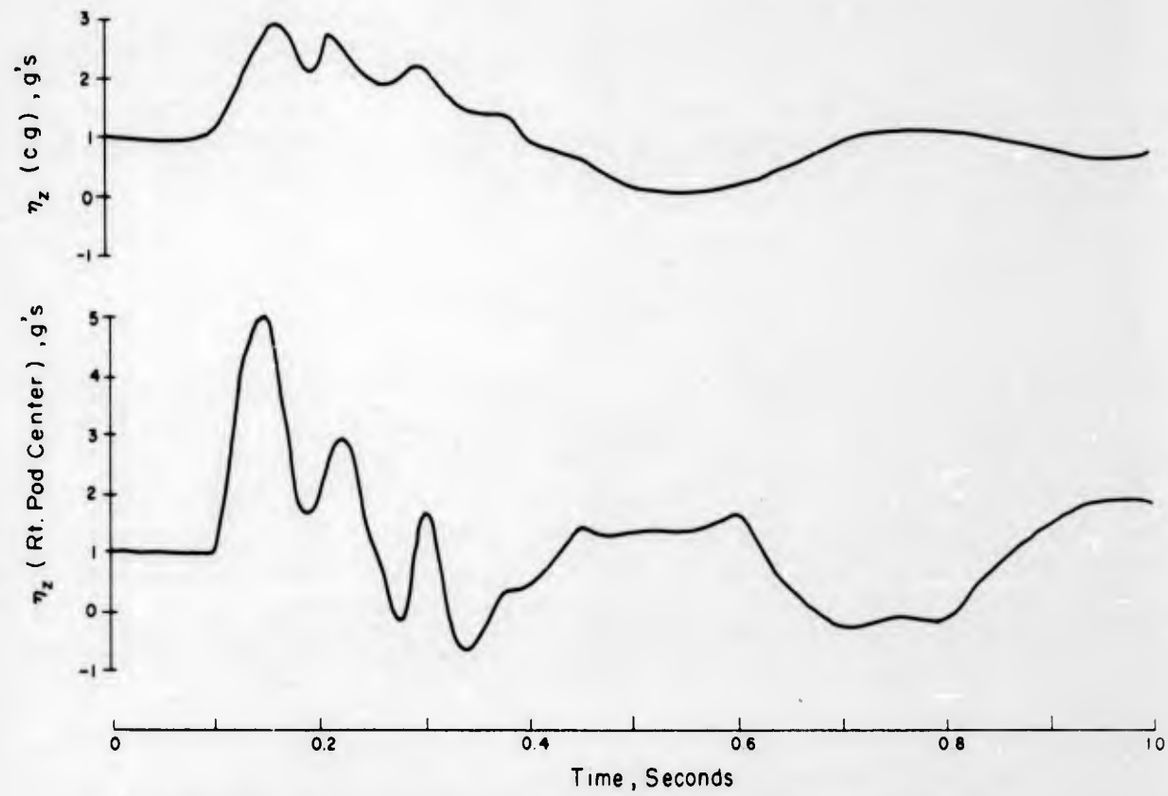

Figure 3.3 Typical vertical accelerometer time histories, Shot Shasta.

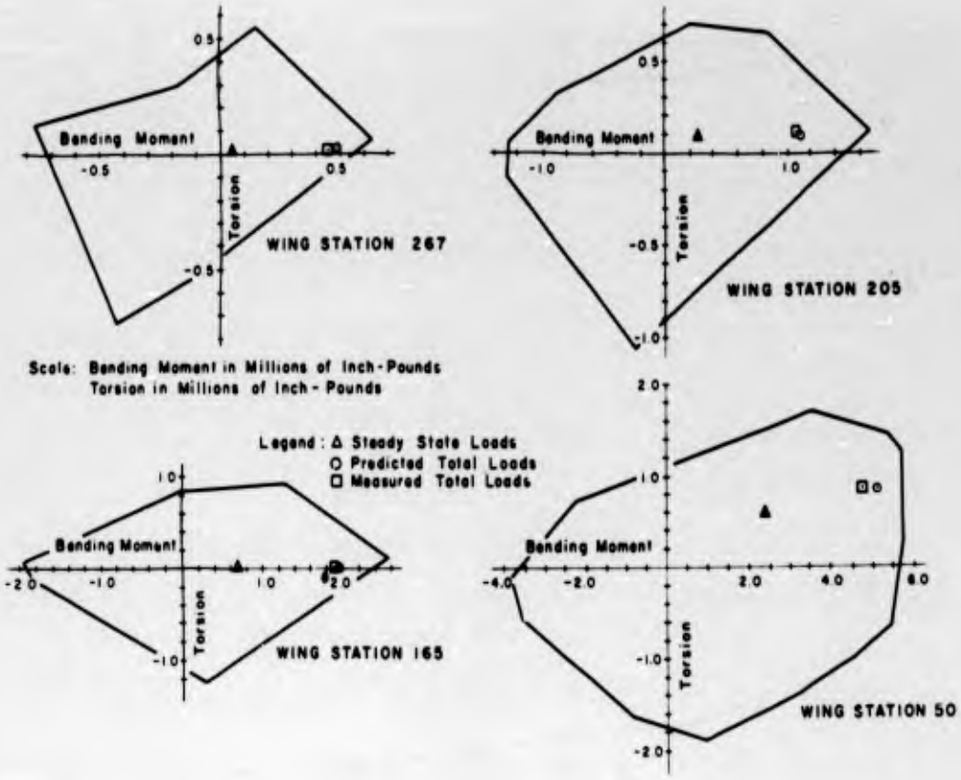

Figure 3.4 Allowable wing load envelopes for bending moment versus torsion, with Shot John loads plotted.

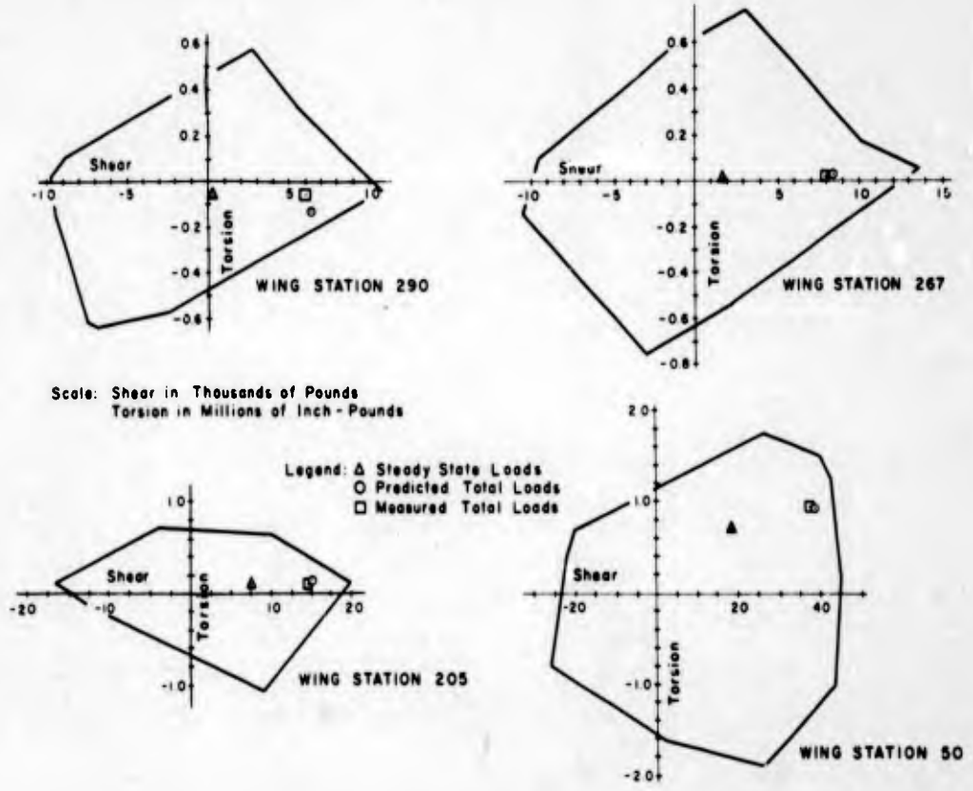

Figure 3.5 Allowable wing load envelopes for shear versus torsion, with Shot John loads plotted.

much lower than had been anticipated and for this reason all future positions inside the triple point path were investigated to assure sufficient damping of wing loads prior to contact with the reflected shock wave. Since the time interval between shock waves for the Shot Wilson event would not allow sufficient damping of the structural dynamic loads, a position outside the triple point path was selected.

For this participation, an aircraft speed of Mach 0.765 and an altitude of 17,000 feet were desired, using the same weight configuration utilized in the previous tests. An aircraft position outside the triple point path was determined to yield an 80 percent of design limit load in the wing tip area.

The horizontal range required to stay outside of the triple point path of the expected yield resulted in a gust-impingement angle less than 45 degrees to the wing chord plane. With this impingement angle, it was decided that diffractive loading would not be significant and therefore the structural response due to gust only was considered. The unit

TABLE 3.9 PEAK WING LOADS, SHOT BOLTZMANN

Wing Station	Predicted Peak Loads *		Measured Peak Loads	
	Load Combination †	Percent Limit Load	Load Combination †	Percent Limit Load
		pct		pct
50	V-T	51	V-T	69
	T-BM	68	T-M	56
205	BM-T	43	BM-T	64
	V-T	46	V-T	57
267	BM-T	43	BM-T	84
	T-BM	61	T-M	20
290	V-T	48	V-T	81
	T-V	52	T-V	16

* Predicted loads based on final aircraft position and final yields; no diffractive loading; and preshot prediction methods.

† BM: Bending Moment; V: Shear; T: Torque. Peak load shown first.

test loads for Shot Boltzmann were reduced approximately 15 percent to account for diffractive loading, then used to position the aircraft with the positive shear-torsion combination (containing the adjustment factor) at Wing Station 267 controlling the position. The unit loads were also adjusted for the altitude change by the method described for Shot Franklin.

The validity of the recorded shear at Wing Station 267 was still being investigated, since no definite conclusions had been reached. However, because of the questionable aspect of this measurement, it was decided to record the shear bridges at Wing Station 267 separately in this and all future participations to permit the use of separate recorded values in a new load equation, if warranted.

All instrumentation functioned properly in this participation, but the aircraft was approximately 5 seconds late in arriving at the intended position. The discrepancy in the aircraft position and the disparity between the positioning yield and actual yield

resulted in a low load level on the structure. Despite the low load level, sufficient data was obtained to substantiate the Shot Boltzmann results. Measured incident thermal energy and nuclear radiation dosage was negligible.

3.4 SHOT PRISCILLA

Positioning criteria used for Shot Priscilla were the same as those used for Shot Wilson. The critical load combination controlling the position was the peak positive bending moment and corresponding torque at Wing Station 267. In this participation, the desired flight conditions required use of Weight Configuration 2 and an aircraft speed of Mach 0.775. An examination of the time between the incident and reflected shock waves resulted in a position outside the triple point path at an altitude near that used for Shot Wilson. This was a desired position that would yield data to confirm the Shot Wilson results.

Prior to positioning for this event the results of the investigation of the peak positive shear recorded at Wing Station 267 during the Shot Boltzmann participation were reviewed. A spanwise distribution plot of the shear (Figure 3.6), at the time of peak shear

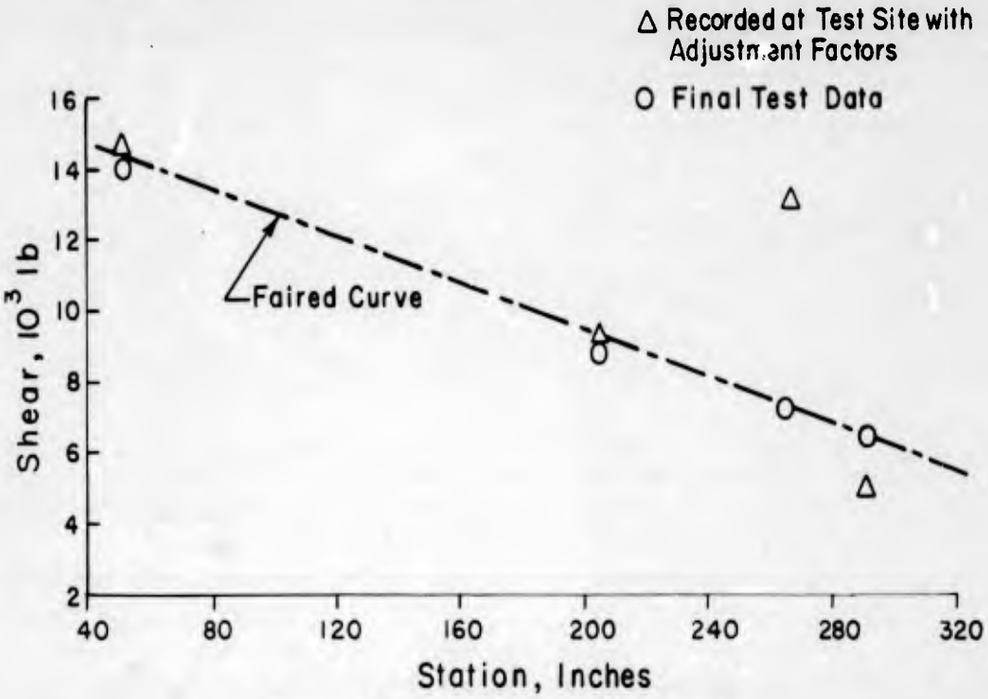

Figure 3.6 Spanwise shear distribution.

at Wing Station 267, appeared unreasonable and could not be justified. The investigation revealed that the load equations used had been developed for steady state loading distributions and a large adjustment factor was incorporated into the constants of the shear equation at Wing Station 267 to account for the effect of high inboard loads. Because of the structural design of the wing, the strain-gages at Wing Station 267 responded to loads applied to the inboard sections in a direction that reduced the response from loads applied outboard of the station. To compensate for the reduction in gage response, an adjustment factor was applied to the shear equation to increase the strain gage reading by 75 percent. The investigation also revealed that the shear equation at Wing Station 290 included an adjustment factor similar to that used for Wing Station 267 except that it reduced the reading by 24 percent.

To evaluate the existing load equations a spanwise distribution of shear similar to that recorded during the Shot Boltzmann participation was established. This distribution was faired through the recorded values at Wing Station 267 and Wing Station 290, eliminating the adjustment factors of .75 and .24 included in the equations, as illustrated in Figure 3.6. The distribution was applied to the load equations with the adjustment factors removed from the shear equations, resulting in shear values which compared favorably with the sample distribution. Based on the results of this examination, it was concluded that the adjustment factors used were unreasonable for the dynamic load distributions encountered and, therefore, were discarded for measurements of loads in all future participations.

Since there was some doubt as to the reliability of the instrumentation at the outboard wing stations, the combined bridges which formed the bending moment equation at Wing Station 267 and shear equation at Wing Station 290 were separated to record individually after Shot Wilson. The shear bridges at Wing Station 267 had previously been separated prior to the Shot Wilson event. This was done in anticipation of a post-test calibration for re-evaluation of the load equations.

Because of the discrepancy between the wing loads recorded in the tests and the analytical values, accelerometers were added to several wing locations to provide additional response data to be used for evaluating and correcting the existing dynamic analysis (Reference 3).

All instrumentation functioned properly except one overpressure gage and one shear bridge. One overpressure trace on the left side of the fuselage and a portion of one shear trace at Wing Station 290 did not record. The aircraft was close to the desired position yielding response data of higher magnitude than obtained in Shot Wilson. The recorded loads data agreed reasonably well with the predicted loads, confirming the results of the Shot Boltzmann and Shot Wilson participations. Measured incident thermal energy and nuclear radiation dosage were negligible.

3.5 SHOT HOOD

The altitude variation between the earlier tests was relatively small; consequently, no firm altitude trend could be obtained. Shot Hood was utilized to determine the effect of altitude on the load response of Weight Configuration 2. The desired aircraft speed was Mach 0.755 for a position yielding 80 percent design limit load.

An analysis was conducted to evaluate the time between the incident and reflected shock wave for a position inside the triple point path, which indicated that the time between the shocks allowed sufficient damping of the dynamic loads from the first shock wave before the aircraft made contact with the second shock wave. Therefore, the desired aircraft position at shock arrival was inside the triple point path at 26,000 feet altitude, tail to ground zero to obtain maximum time between the shock waves.

A study of the time history of the recorded response obtained prior to this event was made to evaluate the effect of diffraction. The recorded time histories agreed closely with the analytical gust (no diffraction) time histories with respect to shape and frequency response. Therefore, from this event on, it was assumed that diffractive loading was either insignificant or did not exist.

Prior to the test it was discovered that the resistance to ground was decreasing for one of the bending moment bridges at Wing Station 165. The strain-gage bridges combined to form the bending moment trace at this station were separated and recorded individually to provide data that could be used in a new load equation if complete failure occurred in the one system.

All instrumentation functioned properly in this event and the test aircraft was in its planned position at shock arrival. Because of the disparity between positioning yield and actual yield, the wing load level was approximately 50 percent of allowable limit load, but the desired altitude effects were obtained. The incident thermal energy recorded was lower than predicted, yet it was the highest recorded value of the test operation. The temperature rise recorded (87 F) was also the highest of the test operation but still too low to produce any significant thermal-stress problem.

3.6 SHOT DIABLO

The four successful participations prior to this event were all at a constant aircraft weight configuration and within the desired Mach number range providing data to evaluate the basic dynamic analysis. Consequently, it was decided to change the aircraft weight configuration for this event to evaluate the effect of the configuration change on the dynamic response. Symmetrical Weight Configuration 3, as described in Table 2.1, was used in this participation. Analysis indicated that the change in mass distribution, due to rockets installed in the tip-pod forward of the elastic axis, affected both the bending and twisting response of the wing.

The desired flight altitude was 19,000 feet with an aircraft speed of Mach 0.755. Since the time between the shock waves inside the triple point path was not sufficient to assure safe positioning, the aircraft was positioned outside the triple point path to be short of ground zero at shock arrival time. The analytical dynamic loads for this configuration in conjunction with the results obtained from the previous tests for Weight Configuration 2 were used to position for 80 percent of design limit load. The critical load consisted of peak bending moment and peak torsion at Wing Station 267, predicted to occur in phase.

One of the strain-gage bridges recording torque at Wing Station 267 failed 0.20 second after shock arrival, the trace of one thermocouple located in the radome was erratic, and the speed of one oscillograph roll was irregular. With these exceptions, all other instrumentation functioned properly and the aircraft was in the desired position at shock arrival. The above malfunctions were corrected prior to the next participation.

Because of the difference in positioning and actual weapon yield and a shift in the phasing of the peak moment and torque loads, the recorded load level was approximately 50 percent of the allowable limit load. The recorded peak loads were in agreement with the predicted loads (adjusted analytical values), and were considered adequate to produce reliable results. Measured incident thermal energy and nuclear radiation were negligible.

3.7 SHOT JOHN

This event consisted of air launching an operational MB-1 weapon from an F-89J aircraft, with the Project 5.5 F-89D flying formation.

The desired flight conditions for the F-89D in this event were an aircraft speed of Mach 0.76 with Weight Configuration 2 at an altitude of 18,500 feet. An additional flight condition was imposed which required the pilot to perform a steady-state 2.2-g turn typical escape maneuver, immediately following launching of the MB-1 weapon. The turn was to be maintained until shock arrival, with tolerances of ± 0.2 g.

The aircraft was positioned to obtain 90 percent of design limit load for the nominal flight conditions and 100 percent of design limit load when positive tolerances were added. Variations in aircraft performance, pilot reaction time, and aircraft load fac-

tors were analyzed to establish reasonable tolerances that would affect the aircraft position at shock arrival. Aircraft performance and pilot reaction time were obtained from data presented in Reference 1 and radar tracking plots recorded on practice missions conducted prior to this event. Rocket-performance test data was also studied to determine realistic tolerance for the analysis.

Precise flight conditions and analysis were required in this event to accomplish the dual purpose of verifying the predicted structural response of the maneuvering aircraft and the predicted nuclear radiation exposure to the air crew. To satisfy both purposes, the test altitude and the rocket time of flight had to be mutually compatible. This was

TABLE 3.10 AIRCRAFT AND ROCKET FLIGHT CONDITIONS, SHOT JOHN

Condition	Desired	Measured
AIRCRAFT		
Roll-in Time, sec	2.5	1.5
Effective Load Factor, g's	2.2	2.25
Angle of Attack, deg	2.2	2.2
Bank Angle, deg	63	57
At Burst Time:		
Degrees of Turn, deg	9	14.0
Pressure Altitude, ft	18,500	18,540
True Airspeed, ft/sec	808	810
Mach Number	0.76	0.759
Height Above Burst, ft	−70	300
Horizontal Range, ft	10,740	−11,000
Offset, ft	130	+300
Slant Range, ft	10,740	11,010
At Shock Arrival Time:		
Degrees of Turn, deg	34	41.0
Launch to Shock Arrival Time, sec	10.45	9.96
Pressure Altitude, ft	18,500	18,560
True Airspeed, ft/sec	812	801
Mach Number	0.76	0.750
Height Above Burst, ft	−70	+320
Horizontal Range, ft	6,680	−6,240
Offset, ft	1,750	+2,570
Slant Range, ft	6,900	6,760
Gust Impingement Angle, deg	48	62
ROCKET		
Horizontal Travel, ft	14,300	13,920
Vertical Drop, ft	500	290
Time of Flight, sec	4.5	4.465

attained by using a pressure altitude of 18,500 feet for launching of the MB-1 weapon and a 4.5 second rocket time of flight.

Since the temperature rise on previous participations was insignificant, the remaining thermocouples were disconnected and the recording channels made available were utilized for recording additional gust response data in this and all later events.

The aircraft trajectory recorded during the test participation agreed closely with the predicted trajectory used for the pretest analysis, as shown in Table 3.10. The

measured wing loads correlated well with the predicted wing loads, as shown in Table 3.11. Figures 3.4 and 3.5 present the comparison of measured total loads with the allowable load envelopes. All instrumentation functioned properly. Measured incident thermal energy was negligible, but the measured radiation dosage was the highest recorded in any one participation during the test operation.

Shot John provided an opportunity to determine whether incremental dynamic loads are affected by the magnitude of the maneuvering loads existing on the structure at shock arrival. The predicted loads for this event, presented in Table 3.11, were based on the unit incremental test loads obtained from level-flight conditions. Since the measured loads agreed with the predicted loads by 6 percent or less at the majority of the stations, it was concluded that the incremental dynamic loads were not affected by the maneuvering loads.

3.8 SHOT KEPLER

Advance planning for both Shot Owens and Shot Kepler included examination of the unsymmetrical weight configuration which also limited the delivery capabilities of the F-89J. The difference between the symmetrical (2) and unsymmetrical (2A) weight configurations is an MB-1 weapon mounted on one wing. The dynamic analysis conducted for Reference 3 indicated this weight configuration produced higher wing loads than Weight Configuration 2. Therefore, evaluation of the true loads experienced by the aircraft in this configuration was quite important.

The aircraft position was established to obtain a critical structural load level of 84 percent at an altitude of 17,500 feet. The desired aircraft speed for this participation remained at Mach 0.755 to minimize the variables affecting the dynamic response. Time between shock waves inside the triple point path was not sufficient to assure safe positioning in this area. Therefore, the aircraft was positioned outside the triple point path to be short of ground zero at shock arrival time. The incremental dynamic loads for the desired position were determined from unit loads derived from previous tests and modified by the ratio of analytical dynamic loads for Weight Configurations 2 and 2A.

One calorimeter which was directed toward ground zero was inoperative in this event and was replaced prior to the next participation. All other instrumentation functioned properly, and the aircraft was in its planned position at shock arrival. The critical wing-load level measured during this test was low in magnitude because of a discrepancy in positioning unit loads and the disparity between positioning yield and actual yield. The unit incremental dynamic loads based on the results of this participation were lower than those for Weight Configuration 2 instead of higher as predicted by the analysis. The wing root (Wing Station 50) experienced the highest percent of design limit load, although the wing tip had been predicted as the critical area. This change in critical wing station was due to the low level of incremental dynamic load and the high level of steady-state load at Wing Station 50. In this participation, the steady-state load represented 50 percent of the total load at Wing Station 50 and 10 percent of the total load in the wing tip area. Measured incident thermal energy and nuclear dosage were negligible.

3.9 SHOT OWENS

Shot Owens was fired on the day following Shot Kepler. The aircraft was positioned outside the triple point path and short of ground zero at shock-arrival time using the method described for Shot Kepler. The short time period between the two events was

TABLE 3.11 GUST RESPONSE, SHOT JOHN

NR: Not Required. NM: Not Measured.

WING STATIONS	WS 50	WS 165	WS 205	WS 267	WS 290
Predicted:					
* Bending Moment, 10^3 in-lb	2,693	NR	858	410	NR
* Corresponding Torsion, 10^3 in-lb	280	NR	7.48	−17.7	NR
Percent Limit Load	89	—	68	90	—
* Shear, 10^3 Pounds	19.7	NR	8.94	7.34	6.225
* Corresponding Torsion, 10^3 in-lb	418	NR	41.8	−17.7	−54.4
Percent Limit Load	90	—	78	77	79
Measured:					
* Bending Moment, 10^3 in-lb	2,400	NM	810	405	NM
* Corresponding Torsion, 10^3 in-lb	265	NM	10	10	NM
Percent Limit Load	84	—	66	83	—
* Shear, 10^3 Pounds	18.3	NM	7.8	6.3	5.2
* Corresponding Torsion	380	NM	40	10	−12
Percent Limit Load	87	—	73	64	62

HORIZONTAL TAIL STATION	HT 13.5
Predicted:	
* Bending Moment, 10^3 in-lb	NR
* Corresponding Torsion, 10^3 in-lb	NR
Percent Limit Load	—
* Shear, 10^3 Pounds	2.43
* Corresponding Torsion, 10^3 in-lb	142
Percent Limit Load	77
Measured:	
* Bending Moment, 10^3 in-lb	135
* Corresponding Torsion, 10^3 in-lb	+35
Percent Limit Load	46
* Shear, 10^3 Pounds	2.2
* Corresponding Torsion, 10^3 in-lb	35
Percent Limit Load	43

FUSELAGE STATION	FS 535
Predicted:	
Horizontal Bending Moment, 10^3 in-lb	68
Corresponding Vertical Bending Moment, 10^3 in-lb	−386
Percent Limit Load	36
Measured:	
Horizontal Bending Moment, 10^3 in-lb	73
Corresponding Vertical Bending Moment, 10^3 in-lb	95
Percent Limit Load	19

* Incremental Loads

not sufficient to permit a reposition for the Shot Owens event based on the Shot Kepler data. In addition, it was not possible to appreciably increase the predicted load level for Shot Owens without exceeding the permissible nuclear dosage. The desired aircraft speed was Mach 0.755 at an altitude of 16,000 feet.

All instrumentation functioned properly and the aircraft was at the planned position at time of shock arrival. The wing loads were low relative to the allowable load envelopes, and the highest percent of design limit load occurred at Wing Station 50. The load magnitude and combinations were approximately the same as experienced during Shot Kepler. Despite the low load level measured in both the Kepler and Owens events, the agreement between the recorded loads of both participations indicated a negligible amount of instrument scatter. Therefore, the results of both participations provided usable data for the unsymmetrical aircraft weight configuration. Measured incident thermal energy and nuclear radiation dosage were negligible.

3.10 SHOT STOKES

Weight Configuration 2A was repeated for Shot Stokes because of the low load levels measured during the Kepler and Owens participations. This decision was based on the need for a test point at a higher load level for verification of the previous results obtained for this weight configuration. The aircraft speed remained at Mach 0.755 at a desired altitude of 15,000 feet.

Because of the burst height above ground, the time between incident and reflected shock waves was sufficient to permit positioning inside the triple point path. The aircraft was positioned to obtain 95 percent of design limit load in the wing-tip area, using unit loads based on the results of both Kepler and Owens. For the desired load level, the predicted aircrew nuclear dosage was prohibitive if the aircraft passed directly over ground zero during or after burst time. To reduce the predicted nuclear dosage to an acceptable level and still obtain the desired load level, the aircraft was positioned with a flight path offset from ground zero. This produced a side and tail component of gust.

The aircraft was in its planned position at shock arrival, receiving approximately 70 percent of the allowable limit load in the wing-tip area. Malfunction of instrumentation included underexposure of the photo panel film, because of an improper setting of the camera lens; failure of the strain-gage bridges at Fuselage Station 480; and failure of the right-hand engine exhaust-gas temperature gage. All other instrumentation functioned properly. Measured nuclear dosage acquired by the pilot and observer was 0.85 rem, considerably lower than predicted analytically.

The maximum design limit load received by the aircraft in this participation was 15 to 20-percent higher than for Shots Owens and Kepler and was of sufficient magnitude to complete the analysis of Weight Configuration 2A. However, the load time histories recorded in the Stokes event showed some response characteristics which did not appear in either the Owens or Kepler results. It appears probable that the side component of gust acting on the wing in this participation was the cause of the difference in response characteristics. Test unit loads for the Stokes event based on the actual aircraft position and measured overpressure were considerably lower than the predicted values based on the previous results of the Kepler and Owens events.

3.11 SHOT SHASTA

This event was utilized to obtain another test point in Weight Configuration 3 with a desired airspeed of Mach 0.755 to evaluate altitude effects and obtain high load response.

A position at 15,000 feet altitude, outside the triple point path, and short of ground zero at time of shock arrival was determined from unit wing loads based on the Shot Diablo results. The effect of altitude on the unit loads was assumed to be the same as indicated by the test results obtained for Weight Configuration 2.

The pressure transducer located on the lower fuselage surface at Fuselage Station 84 was inoperative in this participation, and the wing deflection camera failed. All other instrumentation functioned properly and the aircraft was in the planned position at time of shock arrival.

The maximum percent of design limit load measured was at Wing Station 290 as predicted, and the magnitude of the critical combination correlated well with the predicted values. In general, the wing loads recorded were of a higher magnitude than for most other events. The incident thermal energy measured was low, and the nuclear dosage received by the aircrew was 1.16 rem, considerably lower than predicted.

3.12 SHOT DOPPLER

In this event it was decided to obtain information with respect to side loads on the vertical tail, since this data was considered useful for investigating weapon-delivery techniques other than those presently covered in Reference 1. Aircraft Weight Configuration 2 was used to facilitate correlation with symmetrical loadings.

Shots John and Stokes both included a small side component of gust in the actual tests and therefore provided some test load information concerning the side loads on the vertical tail. This test data was used to position the aircraft in Shot Doppler to obtain 85 percent of design limit load at Fuselage Station 535 for a desired aircraft speed of Mach 0.755 and an altitude of 12,000 feet. The critical load combination consisted of peak side bending moment and corresponding vertical bending moment at Fuselage Station 535 with predicted wing loads at Wing Station 267, equal to 67 percent of the allowable values

All instrumentation functioned properly and the aircraft was in the planned position at shock arrival. The measured loads at Fuselage Station 535 were only 45 percent of the allowable values and the maximum load combination occurring on the wing was 55 percent of the allowable limit load at Wing Station 50. The discrepancy between the measured and predicted loads at Fuselage Station 535 was due to the disparity between the positioning yield and actual yield and the conservatism in the unit loads derived from previous tests.

This event concluded the planned participations to obtain data for evaluating the effects of side gust impingement.

3.13 SHOT FRANKLIN PRIME

The Franklin Prime participation was utilized to obtain data for evaluating altitude effect on the structural response of Weight Configuration 3. The aircraft was positioned to receive a load level of 75 percent of the allowable limit based on the unit test wing loads obtained from the Diablo and Shasta results and extrapolated to the desired altitude. The desired position was at 13,200 feet altitude, inside the triple point path and tail on to ground zero at shock arrival, with an aircraft speed of Mach 0.755.

All instrumentation functioned properly except for one N-9 camera which failed to operate. The aircraft was in the planned position at shock arrival and received approximately 65 percent of allowable limit load at Wing Station 290. Measured nuclear dos-

age acquired by the pilot and observer was 2.44 rems and 2.06 rems, respectively.

The gust input received from participation during Shot Franklin Prime was of sufficient magnitude to evaluate the effect of altitude on the structural response of Weight Configuration 3.

3.14 SHOT SMOKY

The airspeed for all previous participations was in the Mach range of 0.75 to 0.78 where the chord-wise shift in wing center of pressure was negligible. To evaluate the effect of changes in the chord-wise center of pressure, an airspeed of Mach 0.85 was used for Shot Smoky. This airspeed produces the furthest-aft center of pressure for steady-state flight conditions.

Weight Configuration 2 was selected for this event to provide additional data for the most critical weight configuration tested. The aircraft was positioned outside the triple point path, at an altitude of 20,000 feet, and short of ground zero at shock arrival. Analytical unit dynamic loads for this configuration at Mach 0.85 were used in conjunction with previous test results to determine the loads at the desired position. Since this was the first test at this airspeed, the aircraft was positioned to receive 80 percent of design limit load, based on the peak bending moment and corresponding torsion at Wing Station 267.

The aircraft was in the planned position at shock arrival time and all instrumentation functioned satisfactorily except for one N-9 camera which did not operate properly. Useful data for evaluation of the effect of wing center-of-pressure change on the structural response was obtained which again indicated that the analytical data was unconservative. Measured incident thermal energy and nuclear radiation were negligible.

3.15 SUMMARY

To evaluate Weight Configuration 2, four events were utilized to obtain data with the airspeed of the aircraft limited to a Mach range of 0.75 to 0.78. The recorded wing loads at each instrumented wing station were reduced to unit values, using the effective gust velocity (KU_{e_z}) based on the measured overpressure, then plotted versus density altitude for each participation. Curves were faired through the test points to obtain the trend of unit test loads with density altitude, Figures 3.7 through 3.10. The trends exhibited by the test results were consistent, indicating a minimum amount of instrumentation or test scatter. These unit test load curves were used in the positioning analysis conducted for Shot John. The measured loads from Shot John, as shown in Table 3.11, and Figures 3.4 and 3.5, substantiated the validity of the unit load curves developed as explained above and the assumption that the incremental dynamic loads were not affected by the magnitude of maneuvering loads.

Three events, Shots Diablo, Shasta, and Franklin Prime, were used to obtain dynamic response data with rockets installed in the tip pods (Weight Configuration 3) but otherwise maintaining the same general aircraft flight conditions. The results obtained in these three participations showed that the maximum load combinations in this configuration were less critical with respect to the allowable load envelopes than were the loads for Weight Configuration 2.

Three events, Shots Kepler, Owens, and Stokes, were used to obtain dynamic response data for Weight Configuration 2A, basically the same as Weight Configuration 2 except that one MB-1 weapon was installed on the left wing. Contrary to predictions,

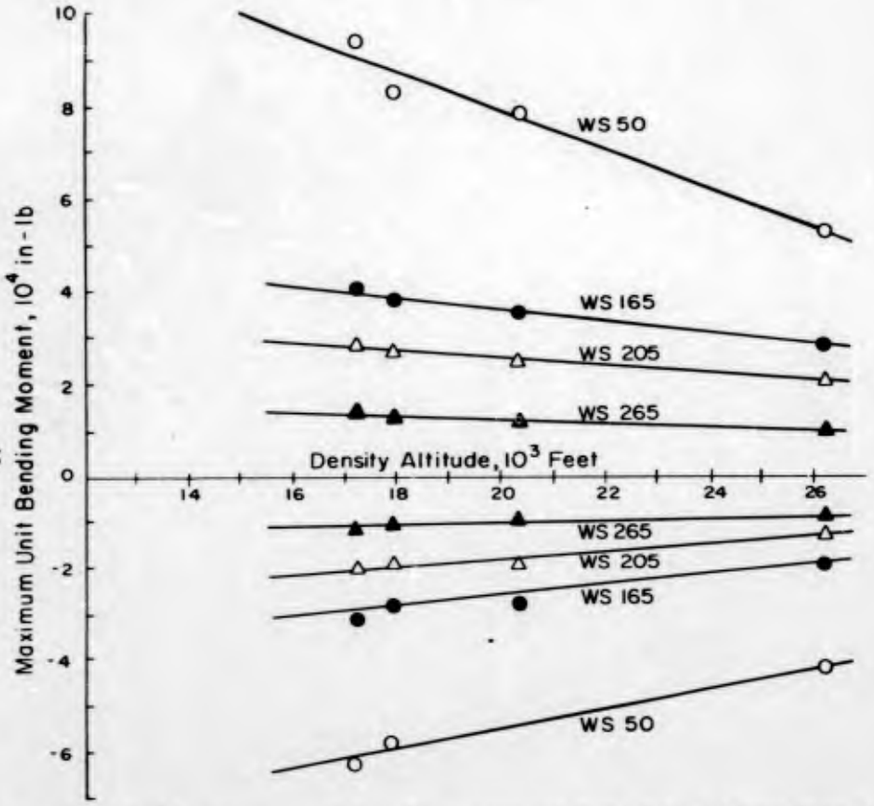

Figure 3.7 Maximum unit bending moment for Weight Condition 2.

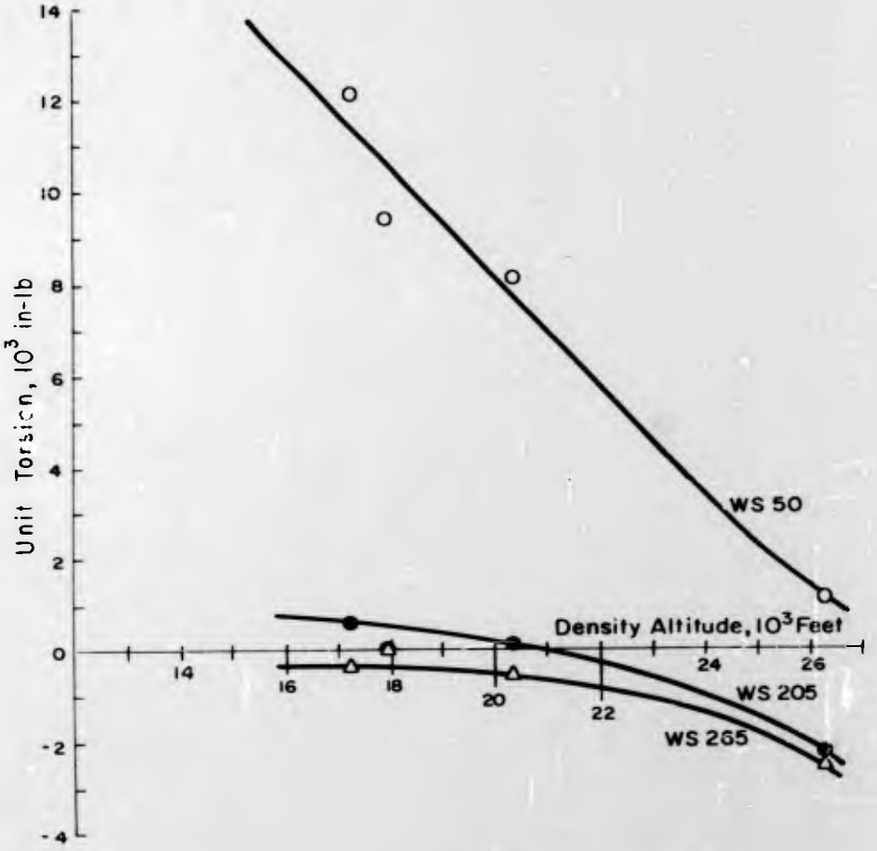

Figure 3.8 Unit torsion at time of peak positive bending moment for Weight Condition 2.

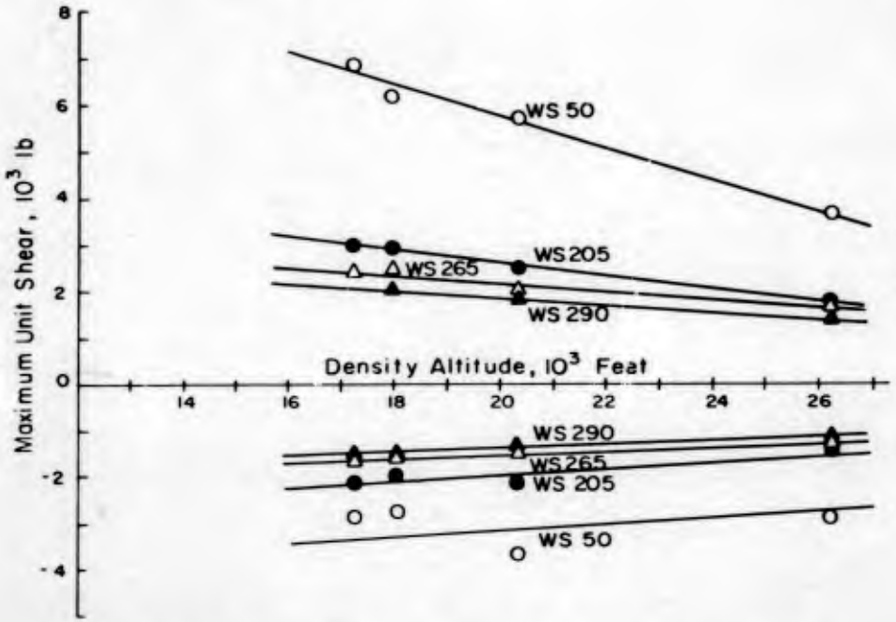

Figure 3.9 Maximum unit shear for Weight Condition 2.

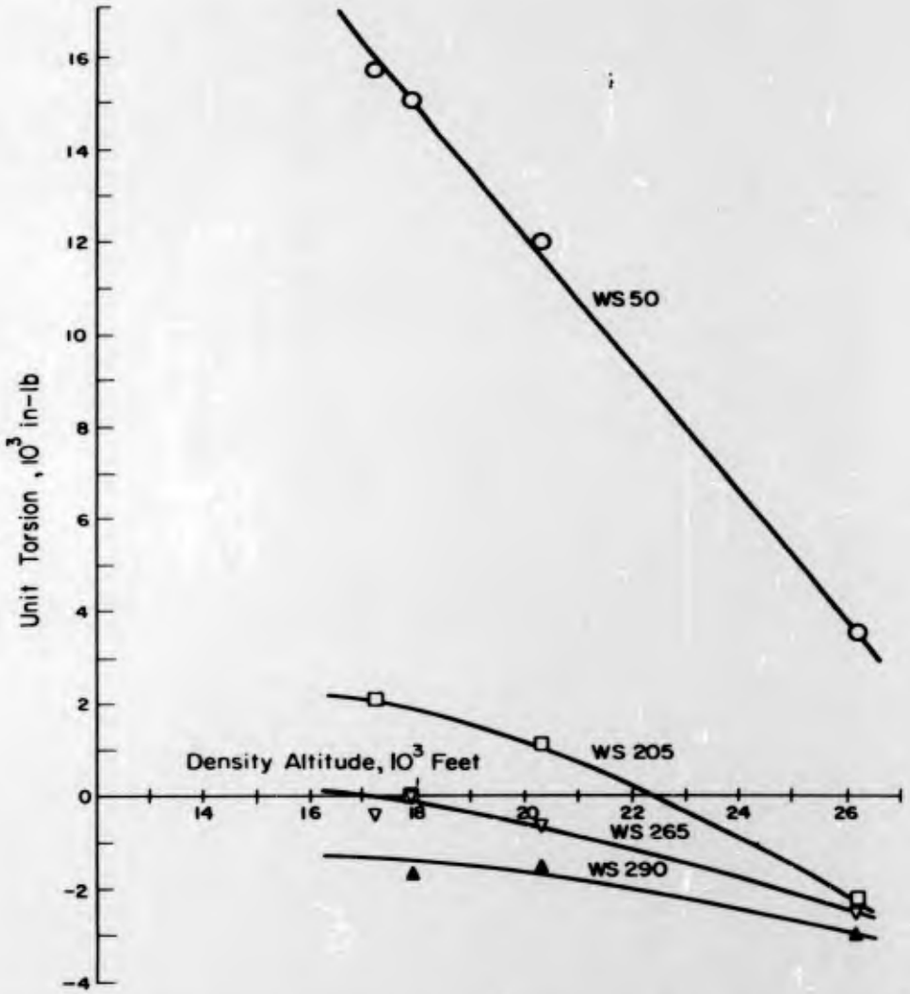

Figure 3.10 Unit torsion at time of peak positive shear for Weight Condition 2.

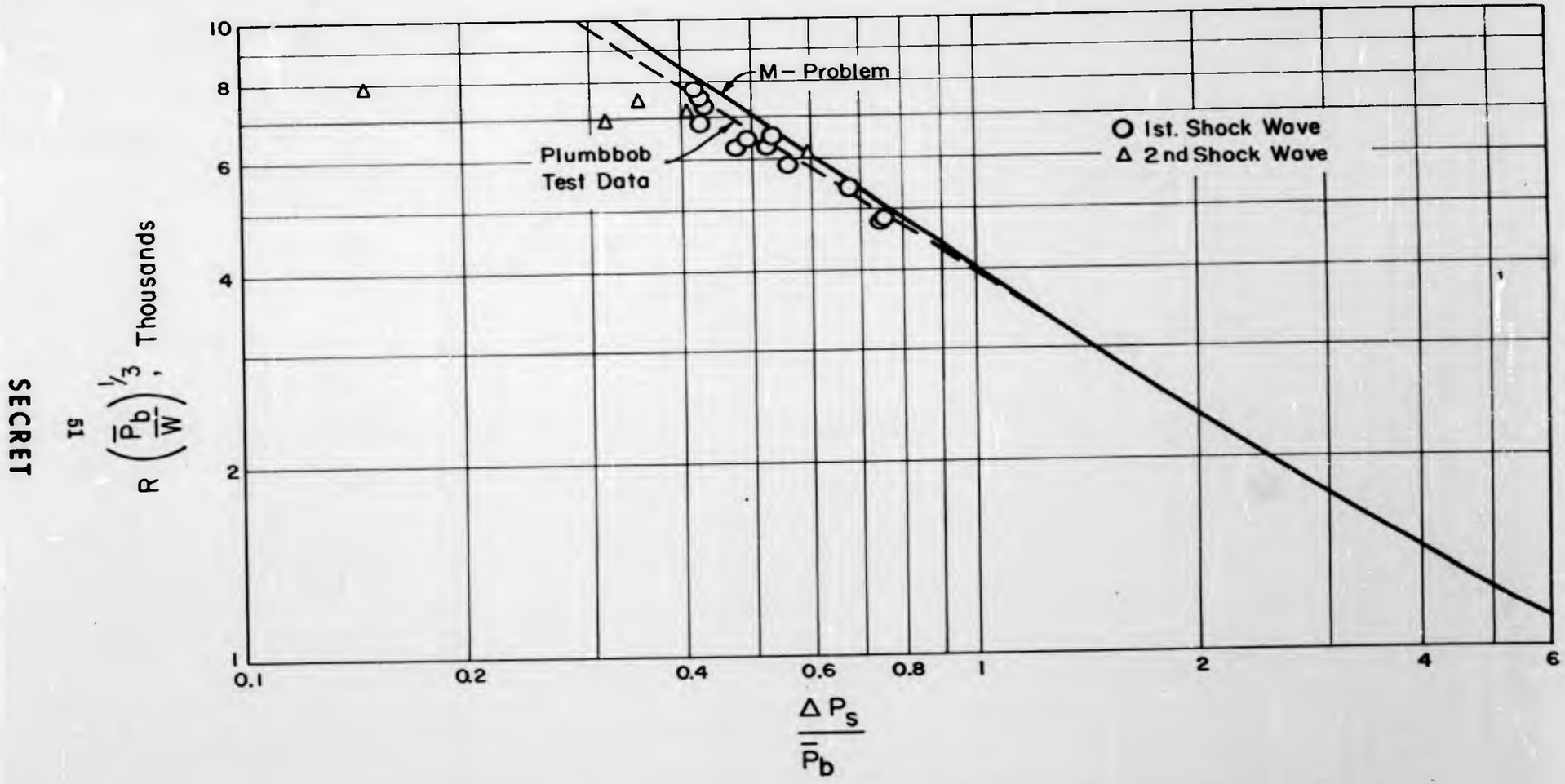

Figure 3.11 Free-air overpressure versus slant-range parameter, based on test results using averaged measured overpressure (Reference 9).

the results obtained in these three events indicated that the maximum load combinations experienced in this weight configuration were less critical than Weight Configuration 2.

Two events, Shots Doppler and Smoky, were used to obtain dynamic response data from side gust impingement and wing center-of-pressure shift, respectively, for Weight Configuration 2. Shot Stokes was used to obtain additional side gust load data for Weight Configuration 2A. This data will be useful for investigation of weapon-delivery techniques not covered in Reference 1 and refinement of the analysis for high speed delivery.

Four pressure transducers were used to determine the overpressure of the shock wave. A faired line on the pressure-time histories was used to obtain the peak overpressure value, as indicated in Figure 3.2. The measured overpressure values for each participation were converted into a plot of free-air overpressure versus slant range. A comparison of the measured free-air overpressure to that based on the M-Problem (Reference 9) is presented in Figure 3.11. The measured values consistently fall below the M-Problem curve.

A study of the time histories of the recorded responses was made to evaluate the effect of diffraction. The recorded time histories agreed closely with the analytical gust (no diffraction) time histories with respect to shape and frequency response. Therefore, it was assumed that diffractive loading was either insignificant or did not exist.

Chapter 4
CONCLUSIONS and RECOMMENDATIONS

4.1 CONCLUSIONS

Sufficient information was obtained during Operation Plumbbob to determine the structural response of the F-89D aircraft in flight to the blast and thermal effects of a nuclear explosion. This data will be used to evaluate the delivery capabilities of the F-89J aircraft.

The dynamic response of the F-89D, and therefore the F-89J, to the blast associated with a nuclear detonation produces higher wing loads than predicted analytically for the F-89J in Reference 1. Therefore, the delivery techniques specified in Reference 1 are unconservative in this respect.

For the conditions tested, the F-89 structural loads result only from the gust associated with the shock wave. Thermal and diffraction effects are so small as to be unimportant.

The horizontal tail and aft fuselage were, in all participations, less critical than the wing. Therefore, the structural limitation is defined by the allowable dynamic loads on the wing structure.

The incremental dynamic loads are not affected by the magnitude of maneuvering loads existing on the structure at shock arrival for the range of flight conditions covered during Shot John.

The use of the M-Problem method for predicting overpressure is slightly conservative, since the recorded overpressure values were lower than predicted by this method.

4.2 RECOMMENDATIONS

No further participation of F-89 series aircraft should be planned for the purposes of determining the aircraft response characteristics.

In order to determine operational weapon-delivery capability of the F-89J, additional data from firing tests of MB-1 rockets would be necessary to confirm safe escape maneuvers.

The dynamic analysis used in the F-89J Capability Study should be reviewed and modified to correct the unconservative limitations that now exist.

REFERENCES

1. "F-89J Weapons System Capability Study"; Phase II, Volume I, Summary, NAI-56-891; Northrop Aircraft, Inc., Hawthorne, California; Secret Restricted Data.

2. Norman P. Hobbs and others; "The Effects of Atomic Explosions on Aircraft; Structural and Aeroelastic Effects"; WADC Technical Report 52-244, Volume III, 1 January 1953; Wright Air Development Center, Wright-Patterson Air Force Base, Ohio; Secret Restricted Data.

3. R. W. White; "F-89J Dynamic Loads Analysis for Blast Input"; NAI-56-185, 7 June 1956; Northrop Aircraft, Inc., Hawthorne, California; Secret.

4. Military Specification, Structural Criteria, Piloted Airplanes, MIL-S-5700 (USAF), 14 December 1954; Confidential.

5. Thomas B. Cook and Carter D. Broyles; "Curves of Atomic Weapon Effects for Various Burst Altitudes"; SC-3282 (TR), 9 March 1954; Sandia Corporation, Albuquerque, New Mexico; Secret Restricted Data.

6. Edwin N. York, Capt, USAF; "Nuclear Radiation from Low Yield Fission Weapons"; AFSWC TN 56-14, December 1956; Secret Restricted Data.

7. "Capabilities of Atomic Weapons"; TM 23-200, November 1955; Armed Forces Special Weapons Project, Washington, D. C.; Secret Restricted Data.

8. R. M. Chapman and M. H. Seavey; "Preliminary Report on the Attenuation of Thermal Radiation from Atomic or Thermonuclear Weapons"; AFCRC TN 54-25, November 1955; Air Force Cambridge Research Center, Cambridge, Massachusetts; Secret Restricted Data.

9. John R. Alexander, Jr., 1/Lt, USAF; "A Modified α Method for Computation of Overpressure and Overpressure Envelopes"; WADC TN WCLS 55-13; Wright Air Development Center, Wright-Patterson Air Force Base, Ohio; Secret Restricted Data.

10. Thomas J. Deegan, Capt, USAF, and Clark G. Fiester, 2/Lt, USAF; "Wright Air Development Center Aircraft Positioning and Tracking"; Operation Redwing Final Report; WADC TN 56-377; September 1956; Secret.

11. James O. Barrett; "Instrumentation and Calibration Report, F-89 Effects Aircraft"; EFT-57-1, February 1957; Northrop Aircraft, Inc., Hawthorne, California; Secret.

12. "A Fourier Integral Method for Obtaining the Sinusoidal Frequency Response from a Unit Step Transient"; FRM 30, 9 March 1949; Flight Research Department, Cornell Aeronautical Laboratories, Buffalo, New York; Unclassified.

13. Aubrey K. J. Gray; "Procedures Manual for Flight Test Determination and Evaluation of Load Distribution and Structural Integrity"; EFT-55-1; June 1955; Northrop Aircraft, Inc., Hawthorne, California; Unclassified.

14. James O. Barrett; "F-89D, Operation Plumbbob Data"; WADC TN 59-28; Wright Air Development Center, Wright-Patterson Air Force Base, Ohio; Confidential.

DISTRIBUTION

Military Distribution Category 52

ARMY ACTIVITIES

1 Deputy Chief of Staff for Military Operations, D/A, Washington 25, D.C. ATTN: Dir. of SW&R
2 Chief of Research and Development, D/A, Washington 25, D.C. ATTN: Atomic Div.
3 Assistant Chief of Staff, Intelligence, D/A, Washington 25, D.C.
4 Chief of Engineers, D/A, Washington 25, D.C. ATTN: ENGTB
5- 6 Office, Chief of Ordnance, D/A, Washington 25, D.C. ATTN: ORDTN
7 Chief of Transportation, D/A, Office of Planning and Int., Washington 25, D.C.
8- 10 Commanding General, U.S. Continental Army Command, Ft. Monroe, Va.
11 Director of Special Weapons Development Office, Headquarters CONARC, Ft. Bliss, Tex. ATTN: Capt. Chester I. Peterson
12 President, U.S. Army Artillery Board, Ft. Sill, Okla.
13 President, U.S. Army Air Defense Board, Ft. Bliss, Tex.
14 President, U.S. Army Aviation Board, Ft. Rucker, Ala. ATTN: ATBG-DG
15 Commandant, U.S. Army Command & General Staff College, Ft. Leavenworth, Kansas. ATTN: ARCHIVES
16 Commandant, U.S. Army Air Defense School, Ft. Bliss, Tex. ATTN: Command & Staff Dept.
17 Commandant, U.S. Army Artillery and Missile School, Ft. Sill, Okla. ATTN: Combat Development Department
18 Commandant, U.S. Army Aviation School, Ft. Rucker, Ala.
19 Commandant, U.S. Army Ordnance School, Aberdeen Proving Ground, Md.
20 Commandant, U.S. Army Ordnance and Guided Missile School, Redstone Arsenal, Ala.
21 Commanding General, U.S. Army Chemical Corps, Research and Development Comd., Washington 25, D.C.
22- 23 Commanding Officer, Chemical Warfare Lab., Army Chemical Center, Md. ATTN: Tech. Library
24 Commanding Officer, Diamond Ord. Fuze Labs., Washington 25, D.C. ATTN: Chief, Nuclear Vulnerability Br. (230)
25- 26 Commanding General, Aberdeen Proving Grounds, Md. ATTN: Director, Ballistics Research Laboratory
27- 28 Commanding General, U.S. Army Ord. Missile Command, Redstone Arsenal, Ala.
29 Commander, Army Rocket and Guided Missile Agency, Redstone Arsenal, Ala. ATTN: Tech Library
30 Commanding General, White Sands Proving Ground, Las Cruces, N. Mex. ATTN: ORDBS-OM
31 Commander, Army Ballistic Missile Agency, Redstone Arsenal, Ala. ATTN: ORDAB-HT
32 Commanding General, Ordnance Ammunition Command, Joliet, Ill.
33 Commanding Officer, USA Transportation Research Command, Ft. Eustis, Va. ATTN: Chief, Tech. Info. Div.
34 Commanding Officer, USA Transportation Combat Development Group, Ft. Eustis, Va.
35 Director, Operations Research Office, Johns Hopkins University, 6935 Arlington Rd., Bethesda 14, Md.
36 Commander-in-Chief, U.S. Army Europe, APO 403, New York, N.Y. ATTN: Opot. Div., Weapons Br.

NAVY ACTIVITIES

37 Chief of Naval Operations, D/N, Washington 25, D.C. ATTN: OP-03EG
38 Chief of Naval Operations, D/N, Washington 25, D.C. ATTN: OP-75
39 Chief of Naval Operations, D/N, Washington 25, D.C. ATTN: OP-922G1
40- 41 Chief of Naval Research, D/N, Washington 25, D.C. ATTN: Code 811
42- 43 Chief, Bureau of Aeronautics, D/N, Washington 25, D.C.
44- 48 Chief, Bureau of Aeronautics, D/N, Washington 25, D.C. ATTN: AER-AD-41/20
49 Chief, Bureau of Medicine and Surgery, D/N, Washington
50 Chief, Bureau of Ships, D/N, Washington 25, D.C. ATTN: Code 423
51 Chief, Bureau of Yards and Docks, D/N, Washington 25, D.C. ATTN: D-440
52 Director, U.S. Naval Research Laboratory, Washington 25, D.C. ATTN: Mrs. Katherine H. Cass
53- 54 Commander, U.S. Naval Ordnance Laboratory, White Oak, Silver Spring 19, Md.
55 Director, Material Lab. (Code 900), New York Naval Shipyard, Brooklyn 1, N.Y.
56 Commanding Officer, U.S. Naval Mine Defense Lab., Panama City, Fla.
57- 58 Commanding Officer, U.S. Naval Radiological Defense Laboratory, San Francisco, Calif. ATTN: Tech. Info. Div.
59 Commanding Officer, U.S. Naval Schools Command, U.S. Naval Station, Treasure Island, San Francisco, Calif.
60 Superintendent, U.S. Naval Postgraduate School, Monterey, Calif.
61 Commanding Officer, Nuclear Weapons Training Center, Atlantic, U.S. Naval Base, Norfolk 11, Va. ATTN: Nuclear Warfare Dept.
62 Commanding Officer, Nuclear Weapons Training Center, Pacific, Naval Station, San Diego, Calif.
63 Commanding Officer, U.S. Naval Damage Control Tng. Center, Naval Base, Philadelphia 12, Pa. ATTN: ABC Defense Course
64 Commanding Officer, Air Development Squadron 5, VX-5, China Lake, Calif.
65 Director, Naval Air Experiment Station, Air Material Center, U.S. Naval Base, Philadelphia, Pa.
66 Commander, Officer U.S. Naval Air Development Center, Johnsville, Pa. ATTN: NAS, Librarian
67 Commanding Officer, Naval Air Sp. Wpns. Facility, Kirtland AFB, Albuquerque, N. Mex.
68 Commander, U.S. Naval Ordnance Test Station, China Lake, Calif.
69 Commandant, U.S. Marine Corps, Washington 25, D.C. ATTN: Code A03H
70 Director, Marine Corps Landing Force, Development Center, MCS, Quantico, Va.
71 Commanding Officer, U.S. Naval CIC School, U.S. Naval Air Station, Glynco, Brunswick, Ga.
72- 80 Chief, Bureau of Naval Weapons, Navy Department, Washington 25, D.C. ATTN: RR12

AIR FORCE ACTIVITIES

81 Assistant for Atomic Energy, HQ, USAF, Washington 25, D.C. ATTN: DCS/O
82 Hq. USAF, ATTN: Operations Analysis Office, Office, Vice Chief of Staff, Washington 25, D. C.
83- 84 Air Force Intelligence Center, HQ. USAF, ACS/I (AFCIN-3V1) Washington 25, D.C.
85 Director of Research and Development, DCS/D, HQ. USAF, Washington 25, D.C. ATTN: Guidance and Weapons Div.
86 Commander, Tactical Air Command, Langley AFB, Va. ATTN: Doc. Security Branch
87 Commander, Air Defense Command, Ent AFB, Colorado. ATTN: Assistant for Atomic Energy, ADLDC-A
88 Commander, Hq. Air Research and Development Command, Andrews AFB, Washington 25, D.C. ATTN: RDRWA

[redacted]

89 Commander, Air Force Ballistic Missile Div. HQ. ARDC, Air Force Unit Post Office, Los Angeles 45, Calif. ATTN: WDSOT

90- 91 Commander, AF Cambridge Research Center, L. G. Hanscom Field, Bedford, Mass. ATTN: CRST-2

92- 96 Commander, Air Force Special Weapons Center, Kirtland AFB, Albuquerque, N. Mex. ATTN: Tech. Info. & Intel. Div.

97- 98 Director, Air University Library, Maxwell AFB, Ala.

99 Commander, Lowry Technical Training Center (TW), Lowry AFB, Denver, Colorado.

100 Commandant, School of Aviation Medicine, USAF, Randolph AFB, Tex. ATTN: Research Secretariat

101 Commander, 1009th Sp. Wpns. Squadron, HQ. USAF, Washington 25, D.C.

102-104 Commander, Wright Air Development Center, Wright-Patterson AFB, Dayton, Ohio. ATTN: WCOSI

105-106 Director, USAF Project RAND, VIA: USAF Liaison Office,

107 Commander, Air Defense Systems Integration Div., L. G. Hanscom Field, Bedford, Mass. ATTN: SIDE-S

108 Chief, Ballistic Missile Early Warning Project Office, 220 Church St., New York 13, N.Y. ATTN: Col. Leo V. Skinner, USAF

109 Commander, Air Technical Intelligence Center, USAF, Wright-Patterson AFB, Ohio. ATTN: AFCIN-4Bla, Library

110 Assistant Chief of Staff, Intelligence, HQ. USAFE, APO 633, New York, N.Y. ATTN: Directorate of Air Targets

111 Commander-in-Chief, Pacific Air Forces, APO 953, San Francisco, Calif. ATTN: PFCIE-MB, Base Recovery

OTHER DEPARTMENT OF DEFENSE ACTIVITIES

112 Director of Defense Research and Engineering, Washington 25, D.C. ATTN: Tech.-Library

113 Chairman, Armed Services Explosives Safety Board, DOD, Building T-7, Gravelly Point, Washington 25, D.C.

114 Director, Weapons Systems Evaluation Group, Room 1E880, The Pentagon, Washington 25, D.C.

115-118 Chief, Defense Atomic Support Agency, Washington 25, D.C. ATTN: Document Library

119 Commander, Field Command, DASA, Sandia Base, Albuquerque, N. Mex.

120 Commander, Field Command, DASA, Sandia Base, Albuquerque, N. Mex. ATTN: FCTG

121-125 Commander, Field Command, DASA, Sandia Base, Albuquerque, N. Mex. ATTN: FCWT

126 Administrator, National Aeronautics and Space Administration, 1520 "H" St., N.W., Washington 25, D.C. ATTN: Mr. R. V. Rhode

127 Commander-in-Chief, Strategic Air Command, Offutt AFB, Neb. ATTN: OAWS

128 Commander-in-Chief, EUCOM, APO 128, New York, N.Y.

ATOMIC ENERGY COMMISSION ACTIVITIES

129-131 U.S. Atomic Energy Commission, Technical Library, Washington 25, D.C. ATTN: For DMA

132-133 Los Alamos Scientific Laboratory, Report Library, P.O. Box 1663, Los Alamos, N. Mex. ATTN: Helen Redman

134-138 Sandia Corporation, Classified Document Division, Sandia Base, Albuquerque, N. Mex. ATTN: H. J. Smyth, Jr.

139-143 University of California Lawrence Radiation Laboratory, P.O. Box 808, Livermore, Calif. ATTN: Clovis G. Craig

144-146 Essential Operating Records, Division of Information Services for Storage at ERC-H. ATTN: John E. Hans, Chief, Headquarters Records and Mail Service Branch, U.S. AEC, Washington 25, D.C.

147 Weapon Data Section, Technical Information Service Extension, Oak Ridge, Tenn.

148-200 Technical Information Service Extension, Oak Ridge, Tenn. (Surplus)

[redacted]

UNCLASSIFIED